Investigation into the extended capabilities of the new DPS-4D ionosonde

A thesis submitted in partial fulfilment of the requirements for the degree of

MASTER OF SCIENCE

of

RHODES UNIVERSITY

by

NICHOLAS SSESSANGA

December 2010

Abstract

The DPS-4D is the latest version of digital ionosonde developed by the UMLCAR (University of Massachusetts in Lowell Center for Atmospheric Research) in 2008. This new ionosonde has advances in both the hardware and software which allows for the promised advanced capabilities. The aim of this thesis was to present results from an experiment undertaken using the Hermanus DPS-4D (34.4°S 19.2°E, South Africa), the first of this version to be installed globally, to answer a science question outside of the normally expected capabilities of an ionosonde. The science question posed focused on the ability of the DPS-4D to provide information on day-time Pc3 pulsations evident in the ionosphere. Day-time Pc3 ULF waves propagating down through the ionosphere cause oscillations in the Doppler shift of High Frequency (HF) radio transmissions that are correlated with the magnetic pulsations recorded on the ground. Evidence is presented which shows that no correlation exists between the ground magnetic pulsation data and DPS-4D ionospheric data. The conclusion was reached that although the DPS-4D is more advanced in its field of technology than its predecessors it may not be used to observe Pc3 pulsations.

Contents

List of Figures

List of Tables

PREFACE

The experimental work described in this thesis was carried out at Hermanus Magnetic Observatory, Hermanus, South Africa from April 2010 to September 2010 under the supervision of Dr. Lee-Anne McKinnell and Dr. Lindsay Magnus.

These studies represent original work by the author and have not otherwise been submitted in any form for any degree or diploma to any tertiary institution. Where use has been made of the work of others it is duly acknowledged in the text.

Acknowledgements

It is my wish to extend my sincere gratitude and high appreciation to my supervisors Dr. Lee-Anne McKinnell and Dr. Lindsay Magnus for their guidance towards the success of this study.

Thanks to the staff of Hermanus Magnetic Observatory (HMO) for their hospitality, logistical, technical and work support, encouragement during my study.

Special thanks go to National Astrophysics and Space Science Programme (NASSP), University of Cape Town for my Masters degree scholarships.

Thanks to my family for the continuous support since I joined the academic field. Special thanks go to my sister Halima Namakula for being their every step of the way, encouraging words, support and love and from my aunt Yvonne Nakalo Nsubuga and Uncle Gerald Ssonko for their support throughout this academic journey.

Thanks to John Bosco Habarulema and other colleagues who assisted me in many ways to finish up this thesis. Your help is greatly appreciated.

Chapter 1

Introduction

This thesis presents research into the extended capabilities of the new digital ionosonde sounder (DPS-4D) that was installed at the Hermanus Magnetic Observatory (HMO), South Africa (34.4°S, 19.2°E) in 2008. This instrument uses basic radar techniques to detect ionospheric changes, but with more advanced technology than its predecessors. It has three basic modes of scientific measurement, viz the ionogram, drift and passive RF sensing mode. The ionogram mode is used for production of vertical incidence ionograms from which the electron density profile can be derived. The drift mode is used in the detection of multiple echoes and evaluation of their source velocities and the passive RF sensing mode is used in monitoring transmitters of opportunity. However, in this research, great emphasis was put on the use of the drift sounding mode to observe Pc3 pulsations in the ionosphere which are discussed further in chapter 4.

1.1 The ionosphere

The ionosphere is that region of the upper atmosphere composed of a plasma (ionized gas) which resonates at a certain frequency depending on the density of particles present. This region ranges from 90 to 500

km in altitude. This plasma is created when the ultra-violet radiation and X-rays from the Sun strip electrons off the gas molecules to become ions (Kelley, 2009). This mixture of negatively (electrons) charged and positively (ions) charged particles is known as a plasma. Depending on the amount of energy released by the sun (solar emission), particles are ionised at particular altitudes. These ionised particles form a horizontally stratified medium with a Chapman density profile. The different layers formed by these particles are defined by the letters D, E, F1 and F2 in the order of their increasing altitude. The D-region occupies altitudes between 60 and 90 km. The concentration of electrons in this region is comparable to the positive ions concentration. The E-region occupies altitudes between 90 and 140 km. The electron concentration in this region is higher than in the D-region by 2 orders of magnitude. The F1 and F2 layers have electron concentrations of about 2.5×10^5 cm^{-3} and 4.5 $\times$ 10^5 cm^{-3} during solar minimum and maximum respectively. The F2-region shows most irregular spatial and temporal variation (Alperovich and Fedorov, 2007; Walker, 2005). These layers are highly conductive because of the charged particles and can carry electric currents, reflect, deflect and scatter radio waves.

The process of reflecting radio waves depends on the refractive index of the plasma. This depends on the electron density (N_e) and their frequency (f) (Margaret and Russell, 1995). Equation 1.1 shows the relationship between N_e in m^{-3} and f in Hz for an unmagnetised plasma. "k" has a value of 80.5 Hz^{2}m^3 and is defined as $e^2/4\pi\varepsilon_o m$, e is the charge of an electron, m is the mass of the electrons and ε_o is the permittivity of free space.

$$\mu^2 = 1 - (kN_e)/f^2 \tag{1.1}$$

1.2 History of ionospheric sounding

Routine ionospheric sounding started in 1932 at Slough in the United Kingdom (UK), using the frequency change method. The sounding procedure was designed by Appleton and Barnett in their historic experiments in 1924, with a transmitter placed at Windsor Great Park and the receiver at Ditton Park (Bibl, 1998). This experiment involved changing the sounding frequency until the radio waves were no longer reflected by the ionosphere. The maximum frequency at which reflection occurred was called the critical frequency. Using this frequency, the group was able to determine the electron content of the ionosphere. This same principle is still applied today in sounders such as radars, but with more advanced technology.

Based on the same principle as above, Bibl (1998) proposed the first digital ionosonde in 1967. In 1970 the first digitally integrating goniometric ionosonde (Digisonde 128, with 128 indicating the height ranges or complex amplitude samples that would be performed), was produced. Thus began the evolution of Digisonde technology. In 1978 the former was succeeded by the Digisonde 256 and it proved to be very successful during its use in Auroral, Polar and Equatorial areas. In 1990 a highly advanced low power transmitting Digital Portable Sounder (DPS) that could analyze more data simultaneously was produced and installed in many different stations around the world (Bibl, 1998). Based on this family of technology between 2004-2008, the University of Massachusetts Lowell Center of Atmospheric Research (UMLCAR) produced a digitally

Figure 1.1: *DPS-4D*

advanced ionospheric sounding instrument known as the Digisonde model DPS-4D, which is shown in figure 1.1. The "D" stands for digital transmitters and receivers which use the digital up-down converter IC chips, the Graychip GC5016 and Analog devices AD9857, that make use of the classic functions of transmitters and receivers by numeric techniques (Reinisch, 2009).

1.2.1 Ionospheric sounding in South Africa

South Africa has been involved in ionospheric research for over 30 years. Grahamstown (33.3° S, 26.5° E) is the oldest ionospheric station and started sounding in 1973 using a Barry Research chirp sounder (McKinnell, 2007). In 1993 South Africa purchased three Digisondes (Model DPS-4) from UMLCAR which were installed at three locations, viz Louisvale (28.5° S, 21.2° E), Grahamstown (33.3° S, 26.5° E) and Madimbo (22.4° S, 30.9° E). The main aim of these installations was to provide real-time scaled ionospheric parameters which could be used in frequency channel selection for HF communication. In 2008 a new improved Digisonde (DPS-4D), donated by the South African Department of Communications, was

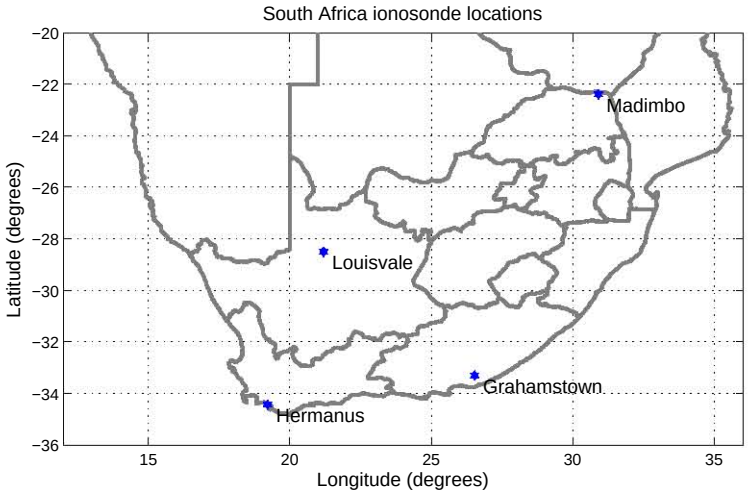

Figure 1.2: *Map showing location of Digisonde Sounders around South Africa.*

included in the network. The installation of the DPS-4D in Hermanus (34.4° S,19.2° E) was the first installation of a model 4D in the world. Figure 1.2 shows the location of the Digisonde stations in South Africa.

1.3 Basic operation of the DPS-4D

DPS-4D is a high frequency (HF) operating radar system used for ionospheric sounding with the main target being the bottom side ionosphere. During operation it transmits a burst of high frequency electromagnetic waves vertically towards the ionosphere for a certain period, switches off its transmitter and "listens" at the receiver for any echoes. If the transmitted frequency is sufficient to drive the plasma at its resonant frequency, total internal reflection occurs and radio waves are reflected back to the receiver. At this point, the refractive index of the plasma approximates zero at a frequency known as the plasma resonance frequency (f_p) given by equation 1.2, where k has the same value as defined in section 1.1 (Reinisch et al., 1998).

$$f_p = \sqrt{kN_e} \tag{1.2}$$

Although equation 1.1 does not show the dependence of the refractive index on the Earth's magnetic field, the presence of the plasma in the Earth's magnetic field brings about wave polarization on the transmitted electromagnetic waves, such that at the receiver two waves are detected, known as the extraordinary and the ordinary wave. These two waves travel at different velocities and appear as two different echoes at the receiver.

Since the ionosphere is full of undulating contours and irregularities, many echoes, the normals of which at the point of reflection are parallel to the wave normals of the incident waves are detected back at the receiver antennas. From the echoes, the amplitude, phase, angle of arrival and polarization are determined. From these variables, a complex spectrum of all the echoes is calculated with all echoes having propagation times less than the pulse width superimposed to form a composite signal at the antennas (Reinisch et al., 1998).

Scanning through the sounding frequencies from 1 MHz to 40 MHz, different points of reflection can be determined and a profile of the ionospheric electron density as a function of altitude can be calculated. This is called the virtual height, which is the height of reflection had the wave continued to travel at the speed of light all the way to the point of reflection.

1.4 Overview

This thesis reports on an investigation into the capabilities of the new DPS-4D installed at Hermanus Magnetic Observatory, South Africa in 2008. In particular, the science question posed to assist with this investigation, and within the scope of Space Physics research undertaken in South Africa, the ability of the DPS-4D to provide data on Pc3 pulsations evident in the ionosphere is investigated.

1.4.1 Organization of the study

Chapter 2 discusses the signal processing involved during transmission and reception of the signals by the DPS-4D.

Chapter 3 discusses the three modes of operation of the DPS-4D, concentrating on the drift sounding mode. Some of the data products that are produced by the different sounding modes are mentioned.

Chapter 4 discusses Pc3 pulsations and their observation using radar sounders and magnetometers.

Chapter 5 explains the design of the experiment using the drift sounding mode to observe Pc3 pulsations. The results from the experiment are also discussed.

Chapter 6 contains the conclusion and proposes the future work that could be done with the DPS-4D.

Chapter 2

DPS-4D signal processing

2.1 Introduction

This chapter discusses the basic signal processing techniques used by the DPS-4D. These techniques have led to noticeable improvements in ionosonde technology, enabling the enhancement of ionospheric measurements, extending the capabilities and leading to more accurate scaling of data. The following are some of the improvements resulting from these techniques;

- 15 dB signal processing gain due to phase-coded pulse compression
- 21 dB additional signal processing gain due to coherent Doppler integration
- Up to 35 dB signal gain due to the RF interference mitigation algorithm
- Electronically switched active crossed-loop receiving antennas
- Frequency multiplexing for improved Doppler resolution

This chapter will explain each of these techniques in detail and their relevance to the subject of this thesis.

2.2 Pulse compression

This technique is used mostly for radar and sonar to augment the range resolution and the signal to noise ratio. It allows the advantages of the sensitivity gain of long pulses to be combined with the fine resolution of short pulses. To increase the length of a pulse, the energy of a single high energetic pulse is spread over the spectrum (Tait, 2009). This pulse then contains more energy without increasing the power. This low power requirement promotes the use of low voltage solid state amplifiers in most modern radars such as the DSP-4D. As the energy of the pulse is spread over the spectrum, its range resolution is reduced in return. To overcome this reduction in range resolution, the pulse is phase-modulated with a code to achieve a bandwidth that is larger than that of an uncoded pulse with the same duration.

It's this augmentation of the range resolution that is of vital importance to this study. The reason is that, in-order to observe Pc3 pulsations at particular altitude, it is necessary to distinguish between two or more targets on the same bearing but at different ranges without intermingling their information.

2.2.1 The spreading code

Since the Dirac delta function has infinite instantaneous power and infinite bandwidth, the choice of selection of the codes to be used during phase modulation depends on their approximation to the ideal case of a perfect delta function (referred to as unit impulse function in signal processing) after the auto-correlation process at the receiver. This function

has a value of zero everywhere except at $x = 0$ where its value integral is 1 as shown below.

$$\delta(x) = \begin{cases} +\infty & x = 0 \\ 0 & x \neq 0 \end{cases} \tag{2.1}$$

or

$$\int_{-\infty}^{+\infty} \delta(x)dx = 1 \tag{2.2}$$

The key to achieving the above delta function lies in the selection of a spreading function, $p(t)$, which possesses an auto-correlation function appropriate for the application. In the DPS-4D, 16-bit complementary series phase codes (1-1-0-1-1-1-1-0-0-1-1-1-0-1-0-0 modulated onto the odd numbered pulses and 0-0-1-0-0-0-0-1-0-1-1-1-0-1-0-0 modulated onto the even numbered pulses) are multiplied by the carrier signal $c(t)$ to give the transmitted signal $s(t)$ in equation 2.3 (Reinisch, 2009).

$$c(t) = exp[j2\pi f_o t]$$

$$s(t) = p(t)c(t)$$

$$s(t) = p(t)exp[j2\pi f_o t] \tag{2.3}$$

These codes comprise a pair of equal and finite length sequences. These have the property that a number of pair like elements within any given separation in one series is equal to the number of unlike pair elements with the same separation in the other (Pearson, 2000). The advantage of using such codes with such symmetry is that their periodic auto-correlation

vector sums up to zero everywhere except at the zero shift. Thus they do not leak energy into any other height bin. For this reason they are to be used in the DPS-4D for vertical incidence measurements.

2.2.2 Timing during transmission

After transmission, some of the signals are reflected back from the E-region. These would obscure the detection of the much weaker echo in a mono-static system. To prevent this, the transmitted pulse must be turned off before the first E-region echoes arrive at the receiver. This is about 600 μs after the beginning of the pulse. Also, since the receiver is saturated when the transmitter pulse comes on again, the pulse repetition frequency is limited by the longest time delay (listening interval) of interest, which is at least 5 ms, corresponding to reflections from 750 km altitude. To meet these constraints, a 533 μs pulse made up of eight 66.67 μs phase-coded chips (15 000 chips/s) is selected, which allows detection of ionospheric echoes starting at 80 km altitude. To avoid excessive range ambiguity, a highest pulse repetition frequency of 200 pps is chosen, which allows reception of the entire pulse from a virtual altitude of 670 km (the pulse itself is 80 km long) before the next pulse is transmitted. This timing captures all but the highest multihop F-region echoes. Under conditions where higher unambiguous ranges, and therefore longer receiver listening intervals, are desired, 100 pps or 50 pps can be selected under software control (Reinisch, 2009; Magnus, 2001).

After transmission, different signals travel different propagation paths between the transmitter and receiver. In this case, the superpositioned received signal, $r(t)$, contains several multi-path echoes delayed by different times in relation to the sent signal $s(t)$. To be precise, the received signal

can be considered as a copy of the transmitted signal $s(t)$ delayed by τ_i times. This can be represented by equation 2.4, where a_i is the amplitude of the i^{th} multi-path component, p is the number of multi-paths and the $\sum$ shows that the received signals sum linearly at the antenna with the phase $\phi_i = j2\pi\tau_i$.

$$r(t) = \sum_{i=1}^{p} a_i s(t - \tau_i) \tag{2.4}$$

Substituting for $s(t-\tau_i)$ from equation 2.3

$$r(t) = \sum_{i=1}^{p} a_i p_i(t - \tau_i) e^{i2\pi f_o(t-\tau_i)} \tag{2.5}$$

$$r(t) = \sum_{i=1}^{p} a_i p_i(t - \tau_i) e^{i2\pi f_o t} . e^{-j2\pi f_o \tau_i} \tag{2.6}$$

$$r(t) = \sum_{i=1}^{p} a_i p_i(t - \tau_i) . e^{[j2\pi f_o t - \phi_i]} \tag{2.7}$$

In the DPS-4D, the phase (ϕ_i) determined at each antenna is detected by a process known as quadrature sampling.

2.2.2.1 Complex down conversion

This is the process of digitizing a continuous (analog) band pass signal and translating its spectrum to be centered on zero. The real and imaginary parts of the spectrum are called the in-phase component (I) and the quadrature component (Q) respectively. Since the discrete digitized signal has to be centered on zero, a complex down conversion is applied to the received time signal by mixing it with $e^{-j2\pi f_o t}$, where f_o is the carrier frequency. This process of multiplying the time signal with either $e^{-j2\pi f_o t}$ or $e^{j2\pi f_o t}$ is known as quadrature mixing and is performed before the sig-

nal is digitized. After the I and Q components are obtained, the phase angle, ϕ, can then be determined as an arc-tangent of the ratio of Q to I. If the ionosphere is fixed, ϕ remains constant, while if the ionosphere is moving the value changes, depending on the Doppler shift frequency introduced by the ionosphere's radial velocity.

When the carrier is stripped off the signal through the process of complex down conversion, the remaining term $r(t)_m$ is left with a complex amplitude $\alpha_i = a_i e^{-j2\pi f_0 \tau_i}$ rather than $\alpha_i = a_i$.

$$r(t)_m = \sum_{i=1}^{p} \alpha_i p(t - \tau_i) \tag{2.8}$$

Because the pulse compression technique is a linear process which does not contribute any phase shifts, the in-phase and quadrature components of $r(t)_m$ can be processed separately (i.e. pulses compressed independently by cross-correlating them with a known spreading code $p(t)$). With this in mind, and having the digitized form of the spreading code function $(p(t))$ and the remaining term $(r(t)_m)$ as $p(n)$ and $r(n)_m$ respectively, the cross-correlation result $r(n)_2$ can then be found by convolving $r(n)_m$ with the impulse response $(h(n))$ of $p(n)$ to give the result in equation 2.9. Where n is the sample number which occurs at time $t = nT$ and T is the sampling interval,

$$r(n)_2 = r(n)_m * h(n) = r(n)_m * p(-n) \tag{2.9}$$

Substituting for $r(n)_m$ and $p(n)$, and writing out the discrete convolution as equation 2.10, the result reduces to a delta function multiplied by a complex amplitude.

$$r(n)_2 = \sum_{i=1}^{p} \alpha_i \sum_{k=1}^{M} p(k-\tau_i)p(k-n) \tag{2.10}$$

$$= \sum_{i=1}^{p} M\alpha_i \delta(n-\tau_i)$$

where k is the auxiliary index used in performing the convolution and M is the number of phase-coded chips. In the DPS-4D, the auto-correlation process is performed by a matched filter which works so as to maximize the signal-to-noise ratio (SNR) of the received signal. After the odd- and even-modulated pulses pass through the matched filter, the final results are added together to give a perfect delta function, hence the term pulse compression.

From the result in equation 2.10, it's clear to see that there is a gain of M in the amplitude at the receiver. In the case of the DPS-4D which uses 16-bit complementary codes, the gain is given by $10 \log (16) = 12$ dB. This gain proves the importance of the pulse compression technique in radar transmission technology. Figure 2.1 shows an example of 4 odd and even pulses, each with amplitude a, passing through a matched filter and later added to give a single pulse with amplitude 8a and a main lobe width of approximately $1/B$, which does not depend on the duration of the transmitted pulse, where B is the phase modulation bandwidth (Reinisch, 2009).

After each pulse compression, the complex amplitude of $r(n)_2$ is placed in the coherent buffer depending on the range that was sampled. However,

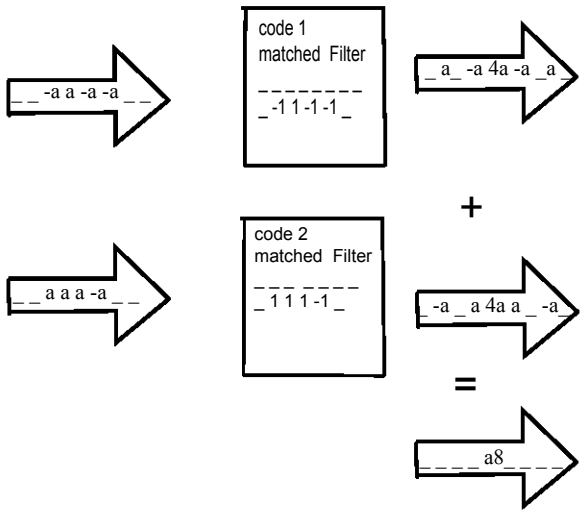

Figure 2.1: *Odd and even complementary codes through the matched filter and then later summed to give a single pulse of high amplitude.*

some of these ranges contain only natural reflections or interference from radio transmitters (noise). To find out whether the range bin contains echo energy from an ionospheric layer, a process known as coherent pulse integration is performed on each range bin.

2.3 Coherent pulse integration.

The term coherent integration can be understood as the time integration of a measured sequence of pulses. For this process to be effective, the time of integration should be limited to the time during which the phase of the signal does not change substantially.

During this process, the SNR is improved by a factor of N_p, where N_p is the number of integrated samples or echoes. As an example, consider a transmitted signal $s(t)$ going through a medium with noise $n_m(t)$. At the receiver, the received signal $y_m(t)$ can be expressed as equation 2.11.

$$y_m(t) = s(t) + n_m(t) \tag{2.11}$$

If this signal is then coherently integrated over N_p samples and the outcome $Z(t)$ normalized over N_p, equation 2.12 shows how greatly the noise is suppressed, thus increasing the SNR of the received signal.

$$Z(t) = \frac{1}{N_p}\sum_{m=1}^{N_p} y_m(t) = \sum_{m=1}^{N_p}\frac{1}{N_p}\left[s(t) + n_m(t)\right] = s(t) + \sum_{m=1}^{N_p}\frac{1}{N_p}n_m(t) \tag{2.12}$$

In the case of a continuously moving target such as the ionosphere, the frequency of the pulses is changed due to the Doppler shift which in turn changes the phase of each sample or echo received. To coherently add these samples, different phase values have to be subtracted from each of the samples so as to obtain coherence. This can be achieved by multiplying the received signal with a unity amplitude phase shift vector and integrating over the transmission period (Magnus, 2001). This process can be viewed as taking the Fourier transform of the received signal as explained below.

Consider N pulses to be transmitted over a frequency, f, the received signal, $R(\tau, t)$, to have amplitude A and angular frequency ω. The received signal can then be expressed as equation 2.13, where τ, is the range time and t is the time between different pulses.

$$R(\tau, t) = Ae^{i\omega t} \tag{2.13}$$

Taking equation 2.13 and multiplying it by a phase shift vector and also integrating it over the observation period, gives equation 2.14 which is the Fourier transform of $R(\tau, t)$ into its frequency domain $F(R)$.

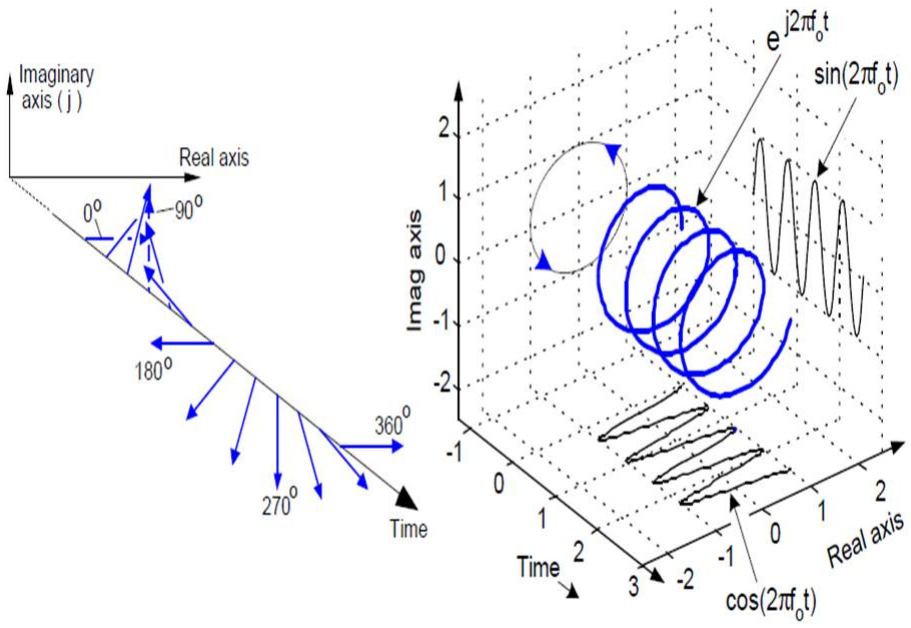

Figure 2.2: *Diagram showing phase as function of time, while keeping amplitude constant.*

$$F(R) = \int_0^T Re^{-i\omega t} dt \tag{2.14}$$

The unity amplitude phase shift factor, e^{-iwt}, that is multiplied with the received signal varies the phase of the received signal as a function of time but keeps the amplitude constant, as shown in figure 2.2 (Magnus, 2001).

In the case of the DPS-4D, where the received signal $R(\tau, n)$ is digitized, the discrete Fourier transform, $F(R)$, is used as shown in equation 2.15, where n is the number of pulses, k is the Doppler line number and N is the total number of pulses transmitted.

$$F(R) = \sum_{n=0}^{N} R(\tau, n) e^{-i\frac{2\pi nk}{N}} \tag{2.15}$$

In the DPS-4D, the period over which a signal in a given range bin is coherently integrated is known as the Coherent Integration Time (CIT). If there is an echo due to a certain ionospheric layer in the bin that is being coherently integrated, the Doppler spectrum ($F(R)$) will have a significant amplitude corresponding to that layer or altitude. It is this Doppler spectrum and phase values for each antenna, each polarization and each frequency that are stored in the DPS-4D memory to be analyzed later.

In terms of gain, the application of coherent integration can lead to an improvement in gain of up 21 dB depending on the integration time. This gain is referred to as the signal processing gain and is given by

$$\text{Processing gain} = 20\frac{S_p/Q_p}{S_i/Q_i}$$

where S_p is the processed signal amplitude, Q_p is the processed noise, S_i is the input signal amplitude and Q_i is the input noise.

2.4 Complex windowing

After the time domain data has been sampled at the receiver, the end samples are so random that a tapering window is used to suppress the spurious response of the Doppler spectrum to below -40dB so as to maintain the spectral resolution (Reinisch, 2009). In the DPS-4D, a Hanning window, $H(n)$, was chosen for this application because of its filtering characteristics, which include a -60 dB side lobe fall-off rate (Oppenheim and Schafer, 1989).

$$H(n) = 0.5 \left\{ 1 - \cos(\frac{2\pi n}{N-1}) \right\} \tag{2.16}$$

In order that the very fine Doppler shifts indicate whether the motion is up or down, the centres of analyzed Doppler lines were altered with a $-1/2$ Doppler line shift that is correct for every value of N (number of samples) required. By choosing a true DFT algorithm and correct Fourier transform coefficients it was possible to make the Doppler lines alterable. To obtain the $1/2$ Doppler line shift, the Hanning function amplitudes were made complex with a phase rotation of 180° and applied by performing complex rather than real multiplications during the entire time domain sampling period NT, where T is the sampling period and N the number of samples.

If each multi-path signal $r(n)$ has only one spectral component such that $k = D_i$, then from equation 2.8 the complex windowed $r(n)$ can then be expressed as

$$r(n) = \left\{ \sum_{i}^{p} \alpha_i \exp\left[-j2\pi\left(nD_i\right)\right] \right\} \mid H(n) \mid \exp\left[-j2\pi(n/2NT)\right] \tag{2.17}$$

$$= \mid H(n) \mid \sum_{i}^{p} \alpha_i \exp\left[-j2\pi\left(nD_i + n/2NT\right)\right] \tag{2.18}$$

2.5 Radio frequency interference mitigation

The inability to operate HF radar systems in noisy RF conditions has been one of the factors hindering the usage of ionospheric sounders in many areas around the world. As the line between "monitoring" and "scientific" ionosonde instruments has been fading, attention has been shifted to new systems such as the DPS-4D, with low power operations, high

measurement cadence, resolution and flexibility (Reinisch et al., 2009). To achieve the former, the DPS-4D had to have a high SNR which would lead to increased rapid measurements. In addition to having a high SNR, the DPS-4D had to operate at a broad bandwidth in order to be capable of measuring reflection altitudes accurately. However, working at a broad bandwidth requires receivers with a wide bandwidth, which comes with the trade-off of more unwanted noise collected along with the signal. This noise is in most cases wide-band background noise and narrow-band interferers. Although there are many methods for removing the background noise in order to increase the SNR, the removal of narrow-band interferers proves to be a challenge, because of their unpredictable occurrence at different frequencies. In order to suppress these interferers in the DPS-4D, a technique known as Radio Frequency Interference Mitigation (RFIM) is applied to the received signal before any other signal processing is done.

When applying the RFIM technique, the discrete Fourier transform (spectrum) of the signal is calculated first. If T is the coherent integration time after digitization, the spectral amplitudes are obtained at integer-indexed frequencies which are multiples of $1/T$. On the other hand, the interferer frequency f_I will not be a harmonic of $1/T$ (i.e. $f_I \neq m/T$, $m = 1, 2, 3, ...$) as shown in figure 2.3. Therefore the interferer will contribute to the neighbouring spectral components with its frequency (f_I) given by equation 2.19.

$$f_I = f_A + \frac{B}{(A+B)T} \tag{2.19}$$

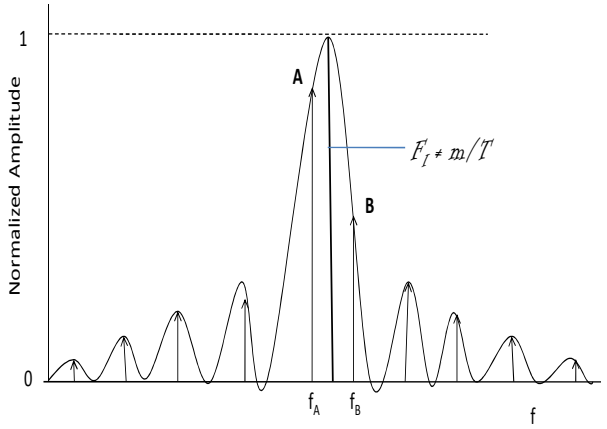

Figure 2.3: *Spectrum of truncated CW signal showing interferer frequency (f_I) not being a multiple of the sampling frequency ($1/T$).*

where f_A is the frequency of the stronger of the two strongest spectral components, and A and B are the spectral amplitudes of the strongest and second strongest respectively.

Since spectral components are numerous in the frequency domain, the best way to subtract the interferer from the main signal is in the time domain. This would require a precise knowledge of the phase and amplitude of the interferer. But since the precise frequency of the interferer is known from equation (2.19), a single line discrete Fourier transformation is used to determine the complex amplitude, C^*, and phase of this interferer.

$$C^* = \frac{1}{N+1}\sum_{n=o}^{N} S_n^* \exp(i2\pi f_I n) \tag{2.20}$$

where S_n^* are the complex signal time samples and N is the total number of samples. Using the inverse transform of equation 2.20 gives the precise time domain (I^*) of the interferer, which can now be easily subtracted from the time domain of the original signal.

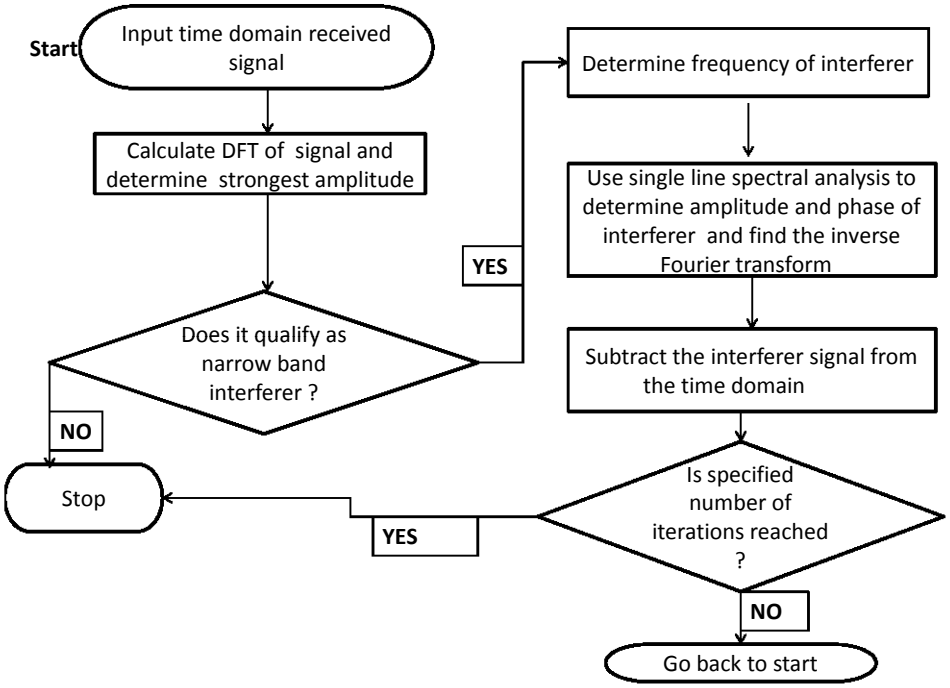

Figure 2.4: *Algorithm showing the steps taken in the radio frequency mitigation process.*

$$I^* = C^* \exp(-i2\pi f_I n) \tag{2.21}$$

This whole process is repeated several times (set by the designer) so that the interferer signals are removed one at a time starting with the strongest. The steps taken in applying this technique are summarized in figure (2.4).

The application of this technique enhances the processing gain by 35dB due to an increase in the signal-to-noise ratio. It's this improvement in the SNR that allows shorter integration times and therefore faster measurements by the DPS-4D.

2.6 Frequency multiplexing

In most previously developed Digisondes, inefficiency was due to a low resolution in time, space and frequency which in most cases are interlinked. To partially overcome this problem in the DPS-4D a technique known as frequency multiplexing was used. In this technique a continuous wave is transmitted and comprises a series of contiguous pulses. These pulses are transmitted at different frequencies in such a manner that they can be separated from each other and from the signal being transmitted. For this reason, it's possible that during sounding the DPS-4D will switch to measuring something else and then come back later and transmit at the same frequency, antenna and polarization combination and fill the second column of the coherent integration buffer, provided the data from the different coherent measurements is not intermingled (Reinisch, 2009). The DPS-4D has 4 antennas and therefore, for each antenna combination one pulse is transmitted while maintaining the same frequency and polarization. If complementary codes are used, 8 pulses have to be transmitted and received for this process to be accomplished.

Frequency multiplexing in the DPS-4D was mainly adopted to increase CIT, which in most cases is required during drift sounding measurements (see chapter 3). To illustrate the effect of frequency multiplexing on the CIT value, consider 8 pulses per frequency to be transmitted over 4 different frequencies ($f1$, $f2$, $f3$, $f4$) as shown in figure (2.5). In the non-multiplexed case, the DPS-4D transmits 8 pulses on $f1$, then transmits another 8 on $f2$, then another 8 on $f3$ and finishes off with 8 on $f4$. However, if multiplexing is applied, different pulses at the different frequencies from $f1$ up to $f4$ are sent and then the process is repeated until the re-

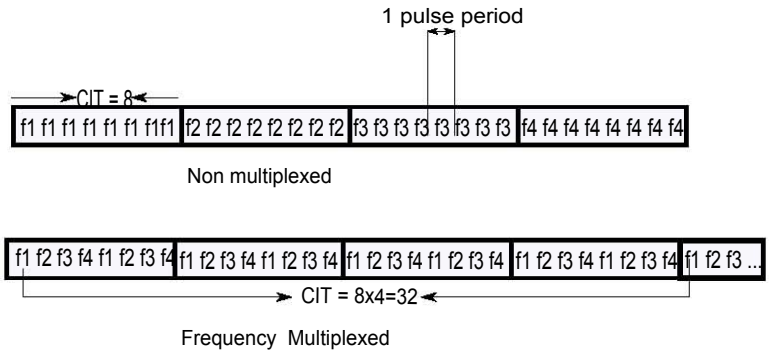

Figure 2.5: *The difference between frequency multiplexed and non-multiplexed transmission, where 8 pulses per frequency are transmitted for the different four frequencies. In the multiplexed case, the CIT value is 4 times greater than in non-multiplexed case, hence increase in the Doppler resolution.*

quired number of pulses for each frequency is exhausted. In both cases, the total number of used pulses is equal to $8 \times 4 = 32$, while the coherent integration time is different. In the case of non-multiplexing, the CIT time is determined by 8 while after multiplexing, the CIT is determined by $8 \times 4 = 32$. This improvement in the CIT time after multiplexing is of great value in increasing the Doppler frequency resolution of the DPS-4D. The parameters that can be used to accommodate frequency multiplexing in the DPS-4D are discussed in chapter 3.

2.7 Antenna array arrangement

The DPS-4D has four receiver antennas, three of which form an equilateral triangle and the fourth placed in the center. Each of these antennas comprises two crossed loops at right angles with each other (rhombic with two orthogonal radiating elements). Under each of the crossed loops is a pre-amp which combines the left- and right-hand circularly polarized

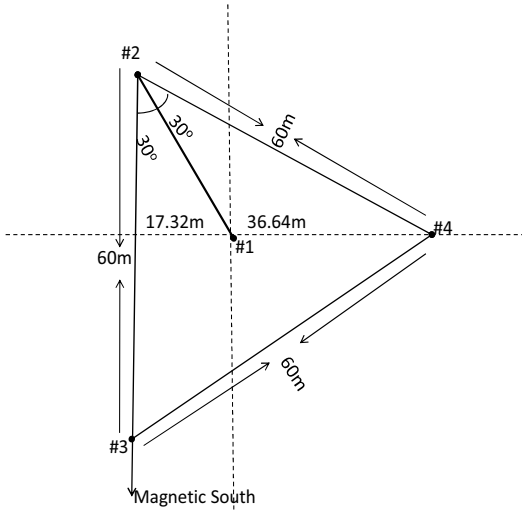

Figure 2.6: *Lay out of the 4 antennas used as transceiver on the DPS-4D.*

waves from the two crossed loops. Figure 2.6 shows the layout of these antennas with their separation distances (Reinisch, 2009).

The distances of 17.3 , 36.64 and 60 m are repeated in six different azimuthal planes, which implies that the phase difference computed for one direction would also apply to the other five directions. This six-way symmetry is exploited by defining the six azimuthal beam directions along the six axes of symmetry of the array, which makes beam-forming very efficient during angle-of-arrival measurements (Reinisch, 2009).

2.8 Angle of arrival measurement

The angle of arrival in ionospheric measurements is used to localise the sources that have been detected. In the DPS-4D two techniques, the aperture resolution technique and super-resolution technique, which utilize the basic principles of interferometry, are used to determine the angle of arrival of the signals received on the four-antenna receiver array.

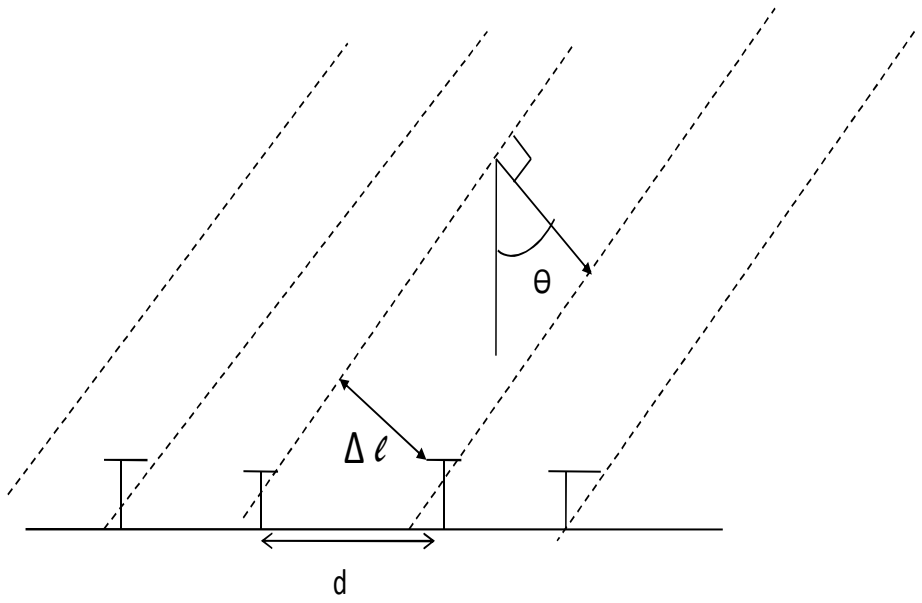

Figure 2.7: *Angle of arrival interferometry.*

2.8.1 Interferometry

Interferometry makes use of phase measurements on each antenna to calculate the angle of arrival. To illustrate this, consider a distant source with zenith angle Θ to be determined, being viewed by an array of receiving antennas separated by a distance d, as shown in figure (2.7). If the phase difference between the antennas is $\triangle\phi$, and the path difference is given by $\triangle l$, then using trigonometry $\triangle l$ can be expressed in terms of d and Θ as shown in equation 2.22.

$$\triangle l = d\sin(\Theta) \tag{2.22}$$

However, the phase difference is given by $\triangle\phi = 2\pi(\triangle l)/\lambda$ which can be expressed by equation 2.23, by substituting equation 2.22 for $\triangle l$, where λ is the free space wavelength of the RF signal.

$$\Delta\phi = (2\pi d \sin(\Theta))/\lambda \tag{2.23}$$

Using the independent phase measurements made on each antenna, and knowing d and λ, equation 2.23 thus solves for the angle-of-arrival.

2.8.1.1 Aperture resolution technique

This technique involves the use of antennas to form different beams through a process known as digital beam-forming. Beam-forming in relation to an array of antennas means optimizing the antenna elements in order to produce the desired beam format as closely as possible. To achieve this, the received signals are weighted with complex coefficients (w_i) using digital multipliers. These complex weights are used to form oblique beams by phase-shifting the four complex amplitudes from the four receiver channels in order to compensate for the additional path length. In general, the DPS-4D can implement complex multiplication for each antenna i, such that if $R_i(t)$ is the complex base band signal onto the antenna, then the complex weighted signal ($R(t)w_i$) would be expressed as equation 2.25, where a_i is the relative amplitude of the weight, ϕ_i is the phase shift of the weight and x_i and y_i are the distances in the East-West and North-South directions respectively as shown in figure 2.8.

$$w_i = a_i e^{i \sin(\phi_i)} \tag{2.24}$$

$$R_i(t)w_i = a_i \{[x_i(t)\cos(\phi_i) - y_i(t)\sin(\phi_i)] + j[x_i(t)\sin(\phi_i) + y_i\cos(\phi_i)]\} \tag{2.25}$$

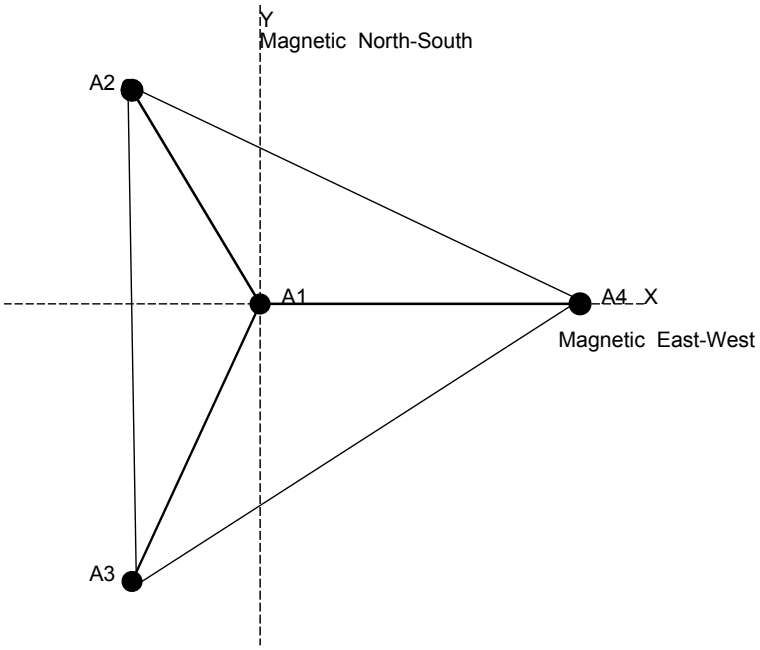

Figure 2.8: *Diagram showing the layout of the antennas with the magnetic North-South and East-West as the Y- and X-axis respectively.*

As a result of the four-antenna array arrangement, a combination of the aperture resolution technique and digital beam-forming can be used to form seven beams from which the beam with the largest amplitude is selected as the best representation of the echo arrival angle.

However, as discussed above, the phase shifts required in summing the echoes into the desired beams depend upon a number of variables, viz:

1. the signal wave length,
2. the antenna geometry (separation distance and orientation),
3. the elevation angle and
4. the azimuth angle.

The above variables are the same as those used in the application of interferometry (subsection 2.8.1) except that more beams were considered this time. To calculate the angle of arrival from the strongest beam indexed j, the phase delay for the antenna resulting from spherical coordinates, (Θ_j,Φ_j), has to be determined, where Θ_j and Φ_j are elevation and azimuth angles respectively. If d'_{ij} is the separation distance from antenna i to antenna 1, where antenna 1 has been taken as the origin ($x_1 = 0$, $y_1 = 0$), then the phase difference ($\triangle\phi_{ij}$), between antenna i's signal and antenna 1's signal, would then be expressed as equation 2.26 with d'_{ij} given by equation 2.27.

$$\triangle\phi_{ij} = (\frac{2\pi \sin\Theta_j}{\lambda})d'_{ij} \tag{2.26}$$

$$d'_{ij} = (x_i \cos\Phi_j + y_i \sin\Phi_j) \tag{2.27}$$

Using the above equation 2.26, and solving for Θ_j, different angles of arrival for the different sources can be determined.

2.8.1.2 Super-resolution technique

Super-resolution is the kind of resolution that is beyond the limit given by the beam width. When applying this technique, the signal phases from the antenna triplet combinations are used to restore the angle direction to the reflecting source in the ionosphere.

When the DPS-4D receives echoes, reflections from different sources may arrive at the same time. In order for the phase of one echo not to be contaminated by another, the sources are isolated with each off-vertical echo having a Doppler shift proportional to the radial velocity (V_r) and $\cos\theta$, where θ is the angle between velocity of motion ($\overrightarrow{V}$) of

the ionosphere and the unit amplitude radial ($\hat{r}$) vector from the station to the ionosphere.

The Doppler velocity in a radar system is the radial component of velocity of a scattering object as observed by a remote sensor. In ionospheric measurements the scattering object is considered to be the ionosphere which is continuously changing with time. To find the expression for Doppler velocity, consider an infinitesimal phase path of the signal to be $\mu(\cos\theta)ds$, where μ is the refractive index of the medium through which the signal travels and θ the angle between the wave normal and the ray direction. If the signal is to move from point A to point B, then the total phase path (P) would be given by

$$P = \int_A^B \mu(\cos\theta)ds \tag{2.28}$$

For a ray traveling in a time-varying medium, the rate of change of the phase path is given by

$$\frac{dP}{dt} = \frac{d}{dt}\left\{\int_A^B \mu\cos\theta ds\right\} + [\overrightarrow{r}.\overrightarrow{v}]_A^B \tag{2.29}$$

such that the Doppler shift in frequency ($\triangle f$) would then be given by equation 2.30, where c is the speed of light and f_R is the sounding frequency.

$$\triangle f = \frac{f_R}{c}\frac{dP}{dt} \tag{2.30}$$

For transmission in a medium with an approximately constant refractive index, the Doppler shift frequency would then be reduced to equation

2.31 which shows how the Doppler shift frequency is related to the Doppler velocity.

$$\triangle f = \frac{f_R}{c}\hat{r}.\overrightarrow{V} \tag{2.31}$$

$$\hat{r}.\overrightarrow{V} =\mid V_r \mid \cos\theta$$

The technique of echo isolation works very well because at a given time the over head ionosphere tends to drift uniformly in the same direction with the same uniform drift velocity. For this reason, the sky can be segmented into narrow bands based on the $\cos\theta$ value which corresponds to a particular range of Doppler shifts. These bands would then indicate at what angle of arrival the Doppler line number should change if the ionosphere is drifting at one velocity (Reinisch et al., 1992).

After multiple sources are separated they are put into their respective range/Doppler bins. However, if multiple sources exist for a particular altitude, they are resolved in the Doppler spectrum computed for that given height. If the resolution is sufficient such that a range/Doppler bin holds signal energy from only one source, the phase information in this Doppler line can be treated as sample of the phase front of a plane wave. Even though many coherent echoes are received from different sources, the energy from one source is represented in the complex amplitude of the Doppler line being processed. This is because the angle of arrival measurement which is done by interferometry does not assume multiple wave interferences.

After isolating sources in their different ranges and Doppler shifts, the interferometry technique can then be used to determine the angle of arrival of each source.

The use of the above two techniques in the DPS-4D has makes it possible to accurately determine the angle of arrival in ionospheric measurements.

2.9 Summary

In this chapter the following signal processing techniques as applied/used by the DPS-4D were discussed:

- Pulse compression
- Coherent pulse integration
- Radio Frequency Interference Mitigation
- Frequency multiplexing
- Angle of Arrival measurement using the super-resolution and an aperture resolution technique

Compared to previous Digisonde models, these techniques have led to improved performance of the DPS-4D namely, improved gain, Doppler resolution and accuracy during sounding.

The next chapter covers the operation of the DPS-4D and also the data products that can be obtained.

Chapter 3

DPS-4D operation

3.1 Introduction

The DPS-4D can perform different measurements depending on the set parameters in its control software known as the Digisonde Commanding and Acquisition Remote Terminal (DCART). These parameters are grouped to form a programme which is responsible for the hardware commanding and data acquisition steps. Up to 256 active programme definitions can be kept in the memory of the DPS-4D (Reinisch, 2009). This chapter describes the functions of each of the different parameters as well as the different measurements that can be performed by the DPS-4D.

3.2 Parameter description

Parameters are variables that can be set to define the mode of operation of the DPS-4D. These parameters are divided into six groups depending on their function while making a measurement. The groups are

1. Frequency stepping
2. Range sampling
3. Pulse integration

Table 3.1: A list of the available parameters and their valid ranges of settings.

Parameter	Abbreviation	Range	Parameter	Abbreviation	Range
Frequency stepping					
Fixed Stepping Law	FSL	0, 1, 2, 3	Frequency Override	FO	-
Fixed Frequency	FF	1 MHz - 30 MHz	Fine Frequency step	FFS	-
Fixed Frequency Repeats	FFR	0 - 15	Fine Step Multiplexing	FSM	-
Number of Fine Steps	NFS	0 - 8			
Range sampling					
Start Range	SR	0 - 1279 km	Inter-Pulse-Period	IPP	N*5 ms, N = 1, 2, 3 ...
Number of Samples	NS	256, 512			
Pulse integration					
Number Integrated Repeats	NIR	8 - 128 (in drift mode)	Inter-pulse Phase Switching	IPPS	-
System settings					
Constant Gain	CG	0 - 3	Rx Gain	RxG	0 - 7
Auto Gain Control	AGC	0 - 2	Wave Form	WF	0, 1
Polarization	Pol	-			
Data processing					
Final Processing Step	FPS	0 - 3	RFIM	RFIM	1 - 99
channel EQ	CEQ	-	Data Reduction Window	DRW	
Number of Best Ranges	NBR	NS/NIR - 32			
Output files					
Out Put Files	OPF	0, 1	Save Product file	SPF	-

4. System settings
5. Data processing
6. Output files

A description of each parameter within the different groups is given below. Table 3.1 shows the abbreviation and range of each described parameter.

3.2.1 Frequency stepping

This group of parameters deals with frequency settings in the Digisonde before a sounding is started. The parameters include: fixed stepping law, fixed frequency, fixed number of fine steps, fine step multiplexing and frequency override.

Fixed Stepping Law (FSL)

This parameter is used to set the frequency increment type (linear, logarithmic, fixed frequency and flex list) for a sounding. The linear format is used for ionogram measurements where it is required that the frequency increases linearly from the set lower limit to a higher limit. Fixed frequency on the other hand, is used when the Digisonde is required to observe a particular altitude continuously (drift mode). Setting this parameter to "flex list" gives the operator an opportunity to choose the frequencies over which the Digisonde should operate.

Fixed Frequency (FF)

Provided the FSL is set to a fixed frequency, this parameter can be used to set the fixed frequency of operation of the DPS-4D. This frequency can be chosen within the range of 1-30 MHz. Depending on the frequency chosen from this range, the Digisonde can be configured to sound within different ranges or layers of the ionosphere.

Fixed Frequency Repeats (FFR)

This parameter determines the number of repeated soundings the Digisonde has to perform at a fixed frequency within a defined programme. The parameter can only be used if the Digisonde is set to run in drift mode. The number of repeats for this parameter range from 0 to 15. For example,

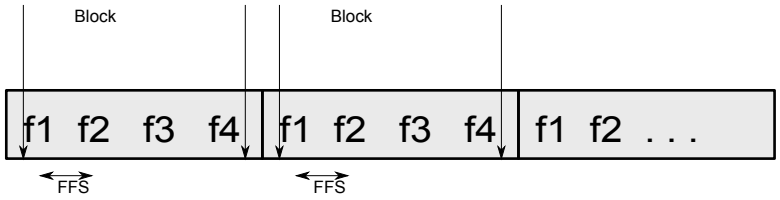

Figure 3.1: *Four frequencies inside a multiplexed block during sounding with FFS as the difference between two neighboring frequencies.*

if a drift measurement is performed at 8 different frequencies (possibly multiplexed) and 4 FFR, then the total number of frequencies is 8*4 = 32. Although this parameter increases the number of spectra, it also increases the exact running time of the programme which in most cases is undesirable.

Fine Frequency Step (FFS)

This parameter defines the size of the frequency increment inside a block of multiplexed frequencies, as shown in figure 3.1 with four frequencies $f1$, $f2$, $f3$ and $f4$. In this case the FFS would be defined as $f2 - f1 = f3 - f2 = f4 - f3$.

Number of Fine Steps (NFS)

This parameter defines the number of frequencies or steps from the previous frequency to the next in a block of multiplexed frequencies.

For example, if the course frequency within a multiplexed block ranges from $f_1 = 2$ MHz to $f_4 = 2.4$ MHz, the number of fines steps using a fine stepping frequency (FFS) of 50 kHz is

$$\frac{f_4 - f_1}{FFS} = \frac{(2.4 - 2) \times 10^6}{50 \times 10^3} = 8$$

Given that the size of the CIT depends on the number of repeated frequencies (as discussed in chapter 2) and that an increase in the NFS value increases the number of frequencies, CIT increases with increasing NFS.

Fine Step Multiplexing (FSM)

The FSM parameter allows the operator to either use frequency multiplexing during a sounding or to disable it. For most drift measurements where high Doppler resolution is needed, frequency multiplexing is enabled in order to increase the CIT value.

Frequency Override (FO)

This parameter sets the Digisonde into an automated frequency override mode. This mode of operation forces the selected fixed frequency (FF) to be shifted up and down in frequency by using data from recent autoscaled ionograms so as to target the F-region of the ionosphere. When this parameter is enabled, the FF set value is ignored by the Digisonde. This kind of operation is used mostly for looking at irregularities within the F-region of the ionosphere.

3.2.2 Range sampling

This group of parameters defines the range within which data should be collected. This parameter group includes the start range, number of samples and inter-pulse period.

The start range parameter defines the range over which the receiver should start sampling, thus it assists the Digisonde to skip ranges where return signals are so weak that they cannot be detected. This parameter is mostly set to 80 km so as to avoid the D-region where absorption is very high during the day thus making it difficult to analyse.

Inter-Pulse Period (IPP)

This parameter can either be used in auto-mode or set manually. It defines the number of pulses per second (pps) to be sent. To avoid receiver saturation during drift sounding, the IPP is assigned specific values, the lowest being 5ms (200pps). For longer listening intervals, this parameter can be set to either 10ms (100pps), 40ms (25pps) or 20ms (50pps). Increasing the IPP increases the overall time during which one spectrum is completed, hence increasing the CIT in return.

Number of Samples (NS)

This parameter determines the number of samples to be made at a particular range. Depending on the chosen number of samples, the inter-pulse period has to be chosen carefully in order to cover the whole range of the total number of samples. For example, if 512 samples (each of range step 2.5 km) are chosen to start from 80 km, the Digisonde chooses an inter-pulse period of 10 ms automatically, equivalent to 1500 km, so that the maximum sampled range of $80 + 512 \times 2.5 = 1360$ km is covered.

3.2.3 Pulse integration

This group of parameters deals with the summing or integration of pulses. The parameters are, number of integrated repeats and inter-pulse phase switching.

Number of Integrated Repeats (NIR)

This parameter defines the number of Doppler spectral lines to be obtained per frequency of sounding and is defined by 2^N, where N is the range value from 3 to 7 in the drift mode. Each NIR contains 2 pulses attributed to the complementary codes used during modulation. For example, if a measurement is made with the NIR being 2^7=128, NFS = 8, FFR =4, IPP = 10 ms and a 16-bit complementary code is used during phase modulation, the number of Doppler spectra lines will be 128, while the number of pulses (NP) needed to complete this measurement will be given by

$$(NP) = 2 * NIR * FFR * NFS$$

$$NP = 2 * 128 * 4 * 8 = 8192$$

provided the frequency multiplexing mode is enabled. The CIT for one frequency in this case is given by

$$CIT = \frac{NP}{FFR} * IPP$$

$$CIT = \frac{8192}{8} * 10 * 10^{-3} = 10.24s$$

With a Doppler resolution (DR) also given by

$$DR = \frac{1}{CIT} = \frac{1}{10.24} = 97mHz$$

If the frequency multiplexing mode is disabled, the CIT and DR value would be given by

$$CIT = \frac{NP}{FFR * NFS} * IPP = 2.56s$$

This clearly shows how frequency multiplexing increases the CIT by NFS times.

Inter-Pulse Phase Switching (IPPS)

This is another way of reducing or removing interferers (noise). In this technique the phase of the odd pulses is flipped by 180° on both transmission and reception so that when the integration of multiple pulses is performed, coherent interferers are suppressed while signals remain enhanced.

3.2.4 System settings

This group of parameters prepares the system for the transmission and reception of signals by adjusting the gain, choosing the type of waveform to be used during transmission and the type of polarization to be stored at the receiver. The parameters in this group include: auto gain control, constant gain, waveform and polarization.

Auto Gain Control (AGC)

Automatic gain control circuits are employed in most systems where the amplitudes of the incoming signals vary over a wide dynamic range. These circuits act so as to maintain a constant level signal output. In the DPS-4D, AGC was acquired because of the sensitivity of the narrow band circuits to the individual RFI sources which change with time and hence are likely to cause an over or under voltage condition. For this reason, all schedules set in the DPS-4D are set with a pre-determined table of automatic gain setting.

Constant Gain (CG)

This parameter is used to set the gain within the antenna switch and tracking filters. Although it does not change during measurements, it can be programmed to change over larger scale changes such as day or night. The variables for this parameter are listed below. Low values are recommended to be used during the night when the D region disappears, leading to less absorption and a strong return signal. The -9 dB in antenna switch and -9 dB in tracker can be combined to give a once off -18 dB gain.

1. Full gain (50 dB)
2. -9 dB in antenna switch
3. -9 dB in tracker.

Wave Form (WF)

This parameter determines the type of waveform to be used during sounding, e.g. a 16-bit complimentary code or 33 μs short pulse wave form. However, the 16-bit complimentary code is preferred for most applications because of its outstanding properties, as discussed in chapter 2.

Polarization (Pol)

After transmission the waves are reflected back. Due to polarization, ordinary (o) and extraordinary (x) waves are observed at the receiver. Depending on the requirements of the measurement, this parameter can be used to save either form of polarization or both. Choosing to observe both polarizations offers an advantage of doubling the CIT, but it increases the amount of data to be stored for that particular programme.

3.2.5 Data processing

This section deals with data reduction and interferer suppression. It acts as the final processing step which determines the type of calculation to be performed on the data depending on the set parameter. The processing steps include: raw data, RFIM, channel equalization application, pulse compression, sum complementary, Doppler calculation and ionogram calculation. If this parameter is set to "raw data", no data reduction or processing is done to the time domain data. This means that the operator has access to the time domain data in raw format. This is one of the improvements of the DPS-4D on the earlier models. "Ionogram calculation" is set for ionogram measurements, while "Doppler calculation" is

used when the drift measurement is carried out with a number of echoes from different altitudes. To reduce the amount of data to be stored, the best "n" ranges are picked for file storage by looking at the strongest echo inter-ranges within a defined window. The n value is set in the DCART software by the operator.

Output files

This parameter defines the output file format after all the signal processing has been completed. To provide for a better structuring of the real-time operations of the DPS-4D, the platform for performing data cleaning and data output is independent of the process which controls the measurements.

Depending on the mode of operation, this parameter can be set to provide different output files e.g. raw data or unprocessed data in the file formats SBF and RSF for ionogram measurements, and DFT for drift measurements. Raw data is processed by an averaging filter and stored as a form of data from all 4 receivers. In this thesis the DFT format was used to acquire the data for the experimental measurements. Therefore, this is the data format that is discussed in more detail here.

DFT format**:** Having chosen the final processing step as a Doppler calculation, the final data is stored in a DFT file. This data file consists of a variable number of 4096-byte blocks with each block consisting of 8-bit amplitude and phase information of the Doppler spectra. The first byte of the first block must always be a recorder type (0x0a). The smallest data entry is a sub-case which contains four Doppler spectra, one obtained at a particular frequency, height gate and polarization setting,

for each antenna. Each Doppler spectrum in a sub-case is 2^Nelements long (Number of Doppler lines in a stored spectrum). For each Doppler spectrum the amplitudes are grouped into 128 elements followed by 128 phase values corresponding to the amplitudes. If a number of height gates is selected for a single frequency (f), all sub-cases for f comprise a height set with simultaneous recordings during one CIT, called a CIT set. If all the sub-cases contained within the 4096 blocks are grouped together, they comprise a case (Reinisch, 2009). Figure 3.2A shows an example of the spectrum and phase for the special case 256.0 km, antenna #1, O-polarization, CIT #1 = 2.56 s, and sub-case 3, extracted from the DFT file using the drift explorer software developed by UMLCAR. On the other hand, figure 3.2B shows the waterfall representation of spectral amplitudes for a group of 4 neighbouring ranges (260-267 km) extracted from antenna #1 data. The waterfall representation assists in illustrating how different spectra for different chosen height gates change.

3.3 Program setting and campaigns

When setting up the different programs to run the DPS-4D uses DCART software. Within the DCART, a schedule is used to coordinate the operation of different programmes. Defining the start and end times of the programmes assists the DPS-4D with an appropriate switching between schedules. There are two ways of calculating the schedule start-up times (SST), namely Rules and Campaigns.

Rules: These are used mostly to start schedules during the day. A rule must have a schedule number and condition. Within the condition one can have, a "start condition" which starts the schedule, "inter-

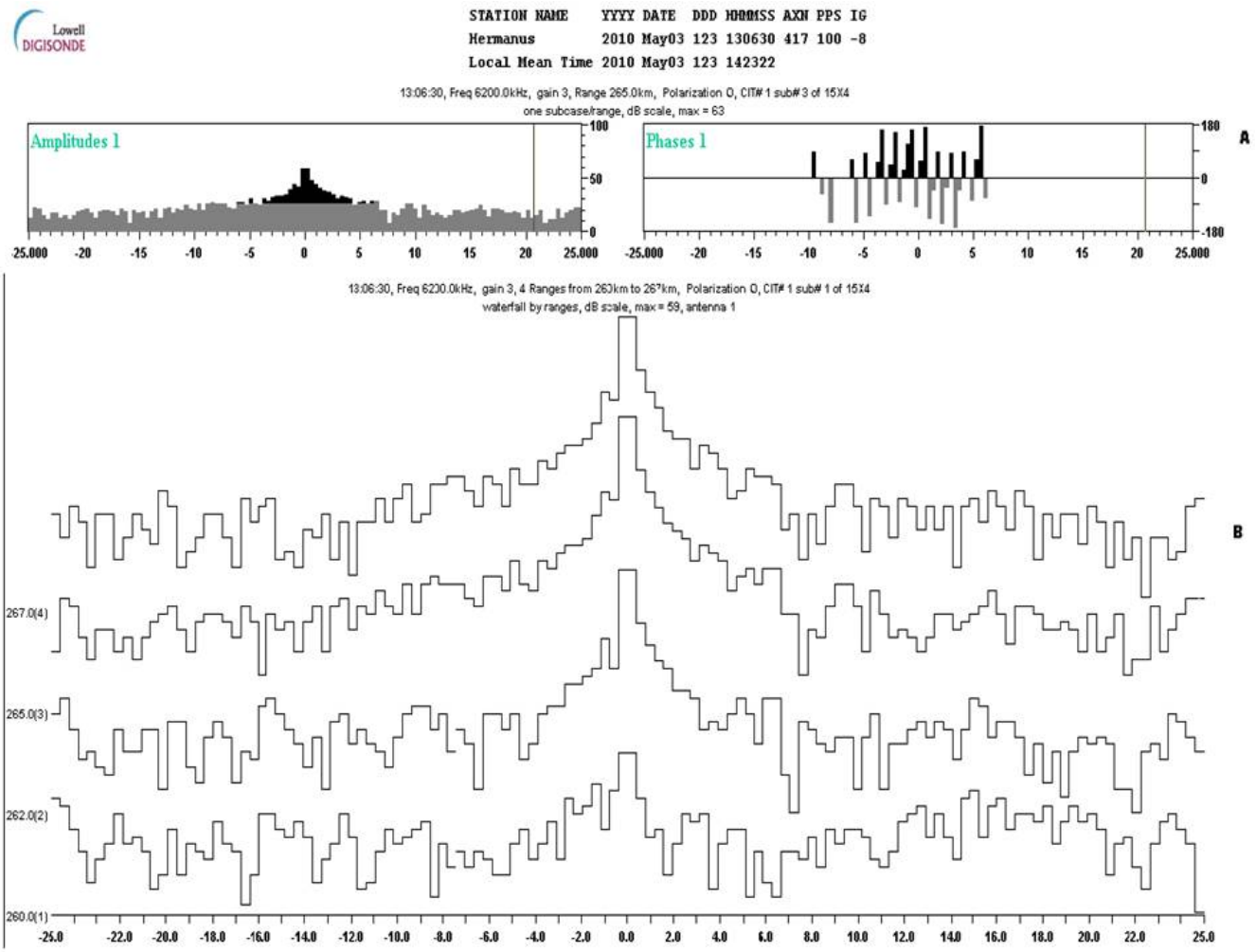

Figure 3.2: *A: Example of representation of spectral amplitude and phase for antenna #1, CIT#1=2.56 s and subcase # 3 extracted using drift explorer. B: Waterfall representation of the 4 chosen neighbouring spectral amplitudes from antenna #1 data, CIT #1= 2.56 s, This example was obtained from the Hermanus station, South Africa.*

val condition" to start and finish the schedule or "default condition" which runs when no other conditions apply. To indicate when these conditions are to be applied, simple formulae with keywords are used as listed below.

- UT (Universal Time) of the day (keywords Start.UT and Range.UT)
- Daylight time in F region (keyword Day with boundary conditions Day.Start and Day.End)
- Night time in the F region (keyword Night and its boundaries Night.Start and Night.End)
- Offset (key word Offset)

Campaigns: Campaign requests would contain schedule numbers, start UT and end UT for the period during which the schedule should run. They are used to override existing SST sequences generated using planning rules. Apart from the campaign requests that are typed into the campaign table manually, the DPS-4D also offers an option of accepting Remote Campaign Requests (RCR files) which in most cases assist in handling a large number of scheduled switches (Reinisch, 2009).

In most cases the schedules set up to run contain the Built-In Test (BIT) programme which evaluates the systems health, cross-channel equalizing programme to calculates which compensation inequalities in receiver

channels and the great gain table programme which refreshes the auto-gain table. The former is placed at the end of the schedule in order to evaluate the current noise before the actual measurements are started.

When using DCART, one can choose the time delay between the programmes, with the default being 1 s. However, if the programme is set to begin "As Soon As Possible" (ASAP, short form used in DCART) the previous one ends. In this case, the fixed offset duration times are not considered and the time is not synchronized to the computer clock any more. This setting is useful if one is doing a continuous observation over long periods of time.

3.4 Scientific measurements

The main purpose of the DPS-4D is to collect and archive data for fundamental scientific research. Scientific measurements, as far as the DPS-4D is concerned, are measurements of the electron density and motion of the ionosphere. The DPS-4D performs several measurements, depending on the optimisation of the parameters. These measurements include:

1. Vertical incidence (VI) ionogram measurements
2. Drift measurement
3. Ionospheric tilt
4. Passive RF sensing mode

3.4.0.1 VI ionogram measurements

Ionograms provide the relationship between the sounding frequency and the range where reflection takes place. An ionogram is basically a

virtual height against frequency description of the ionosphere. The DPS-4D provides different types of ionograms, from vertical incidence measurements and Doppler analysis. The Doppler ionogram provides evaluation of the echo's angle-of-arrival of echoes with multi-beam processing and frequency precision ranging. In addition to vertical incidence, the Digisonde can also provide oblique incidence ionogram measurements which involve transmission between two Digisondes.

To set up the DPS-4D to do ionogram measurements, the sounding frequency has to be set so that it increases linearly with time from the lower limit to the upper limit. As a result of the RFIM technique (discussed in chapter 2), the lower limit frequency can be chosen to begin from as low as 0.3 MHz without worrying about interferers. Figure 3.3 shows the parameters in the DCART software that can be set for a routine vertical incidence ionogram measurement.

When a sounding is performed in an ionogram mode and the Doppler spectra data from pulse compression and coherent integration (discussed in chapter 2) is stored, a technique known as the maximum maximum method (MMM) is used to extract the largest amplitude per height, which is then converted to logarithmic magnitude in dB units. This process is done for each antenna, polarization, and each frequency measured. The data products obtained are then stored in RSF (Routine Scientific Format) or SBF (single Byte Format) depending on the after-use requirements. The ionogram obtained from the RSF data products show echo directions, as opposed to the SBF format which is mostly used when a hardware fault is suspected in one of the receiver channels. In addition to the above, the SBF format can also be used as a way of reducing on the amount

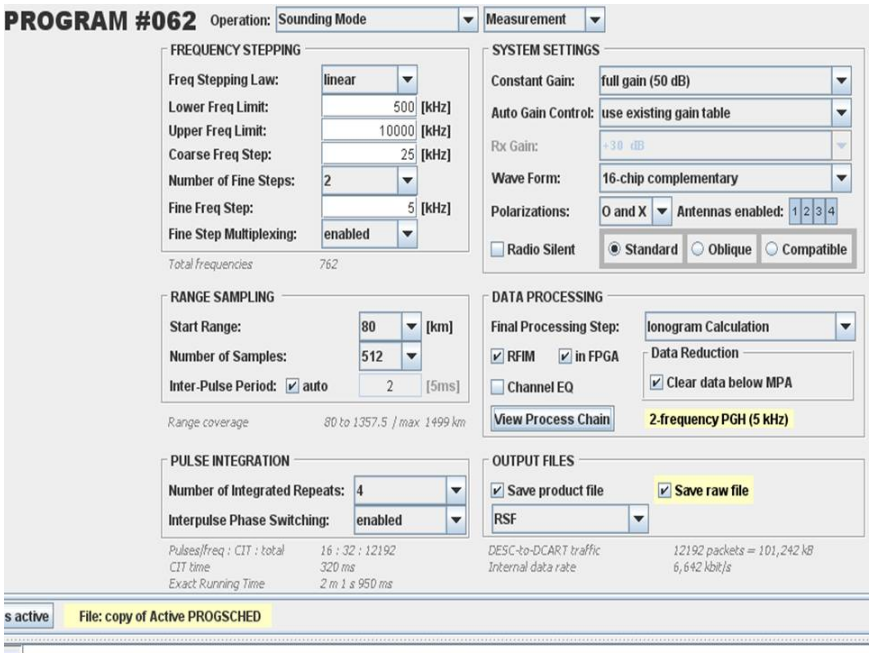

Figure 3.3: *Program 62 in DCART software showing parameters that can be set to run an ionogram measurement.*

of data to be stored. Figure 3.4 shows an ionogram derived from the RSF data formats using version 5 of the Automatic Real-Time Ionogram Scalar with True height (ARTIST 5) software developed at UMLCAR for the analysis of ionogram data. The different colours in the ionogram show the directions of each echo, except for the red and green which represent the O and X modes of polarization respectively.

3.4.1 Drift measurements

Drift measurements show how a particular height of the ionosphere changes with time. To do a drift sounding, a fixed frequency over which the Digisonde is to operate, has to be chosen so as to define the height or range of interest. Figure 3.5 shows other parameters that can be optimised to meet different drift measurement requirements.

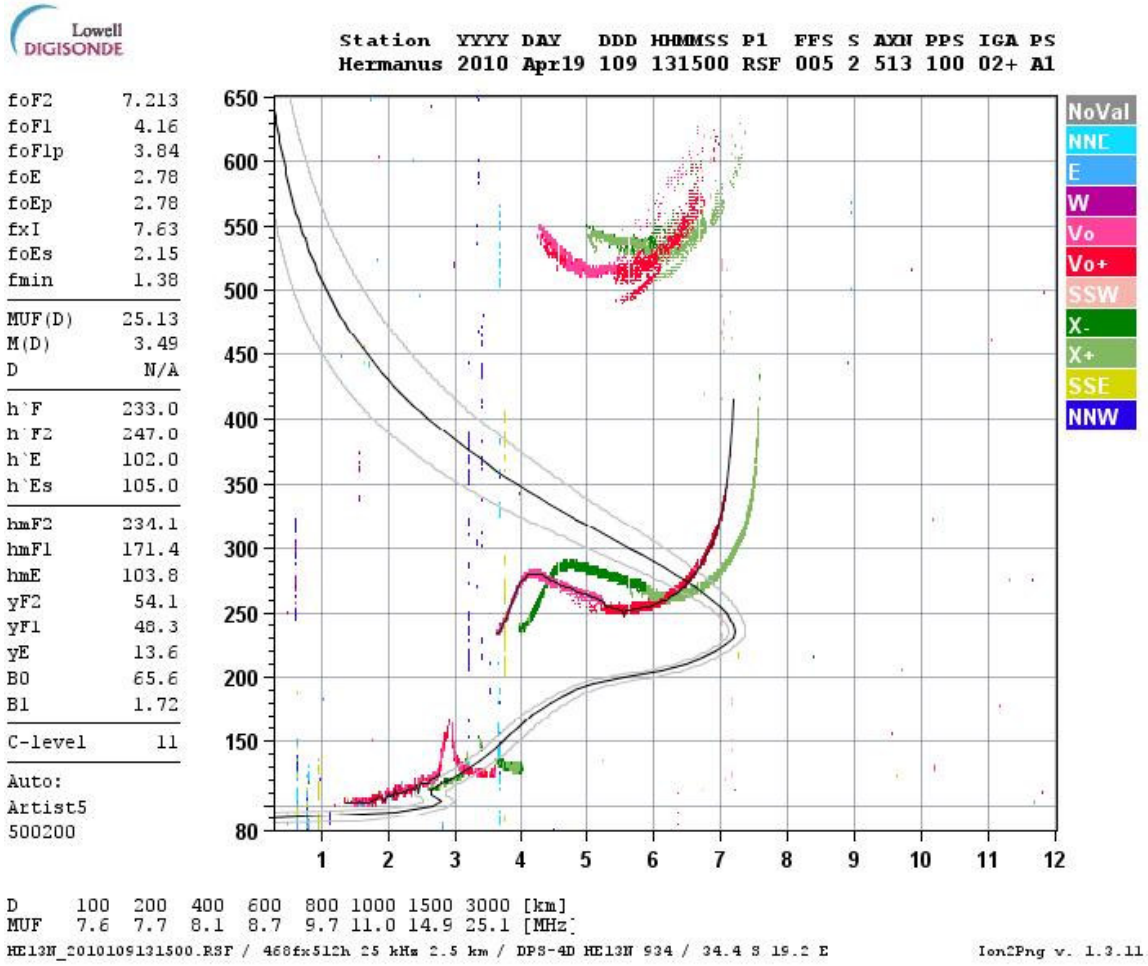

Figure 3.4: *Ionogram showing electron density profile derived from RSF data at the Hermanus Magnetic Observatory, South Africa.*

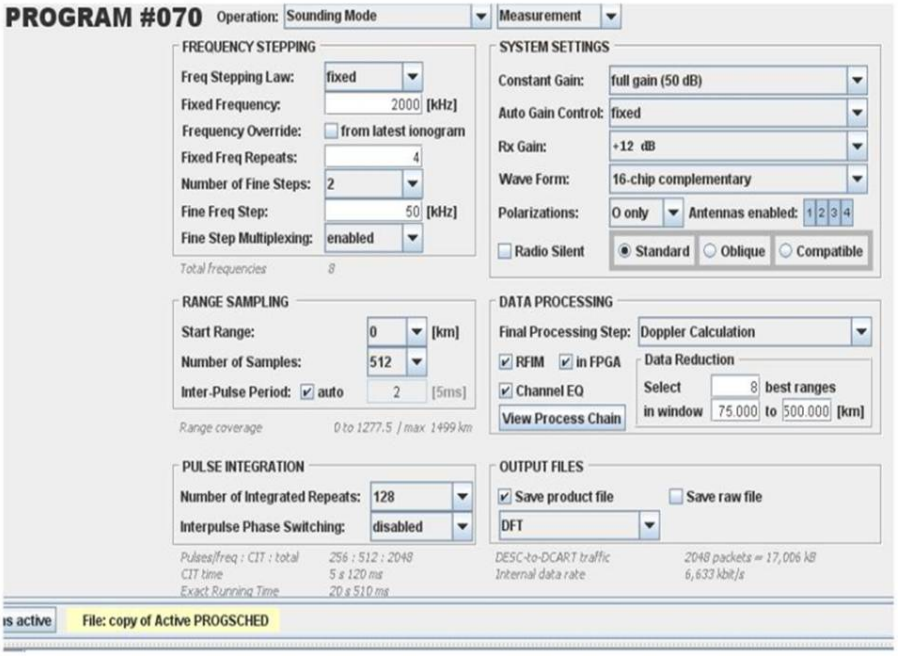

Figure 3.5: *Parameters for drift sounding measurements.*

Although most of the parameters used in drift sounding look similar to those used in ionogram measurements, there are small differences, such as the high Doppler frequency resolution which requires the number of pulses per frequency (i.e., number of frequencies per spectrum) to be as high as possible so as to cover a sufficient range of the Doppler frequencies due to ionospheric irregularities. The other difference is that in the drift mode, the Doppler spectra are computed for each height, antenna, polarization and frequency and stored in the DFT file together with their corresponding phase. As a result, drift measurements always produce a large volume of data for storage. From these DFT files data is later extracted for other

data products such as Doppler skymaps, drift velocities and ionospheric tilt.

3.4.1.1 Doppler skymap

After the sources are separated according to their Doppler frequencies, their zenith and azimuth arrival angles are determined using an interferometry technique (discussed in chapter 2). A graphical map representing these sources and illustrating the angle-of-arrival and Doppler shift is what is known as a Doppler skymap. In the DPS-4D, the DFTSky software is used to extract data from the DFT files, from which the sources are determined and stored in SKY output files and then plotted, using the SKY2PNG software. Figure 3.6 shows a skymap produced by the Hermanus Digisonde station (34.4°S 19.2°E), South Africa. The Doppler shift frequencies are distinguished from each other by the different colours of the plotting symbols.

3.4.1.2 Drift velocities

After each of the sources is located in the ionosphere, the bulk velocity (drift velocity) of the ionospheric structure over the sounder can be determined with an assumption of bulk motion of the plasma. If i is the index representing the i^{th} source with Doppler shift frequency $\triangle f_i$, azimuth angle θ_i, zenith angle ϕ_i and $\hat{k}_i$ the vector perpendicular to the ray path, then the equation for the Doppler shift frequency of source i is given by

$$\triangle f_i = \frac{2}{c}(\hat{k}_i.\overrightarrow{V})f_R \tag{3.1}$$

where

$$\hat{k}_i.\overrightarrow{V} = \sin\theta_i\cos\phi_i V_x + \sin\theta_i\sin\phi_i V_y + \cos\theta_i V_z \tag{3.2}$$

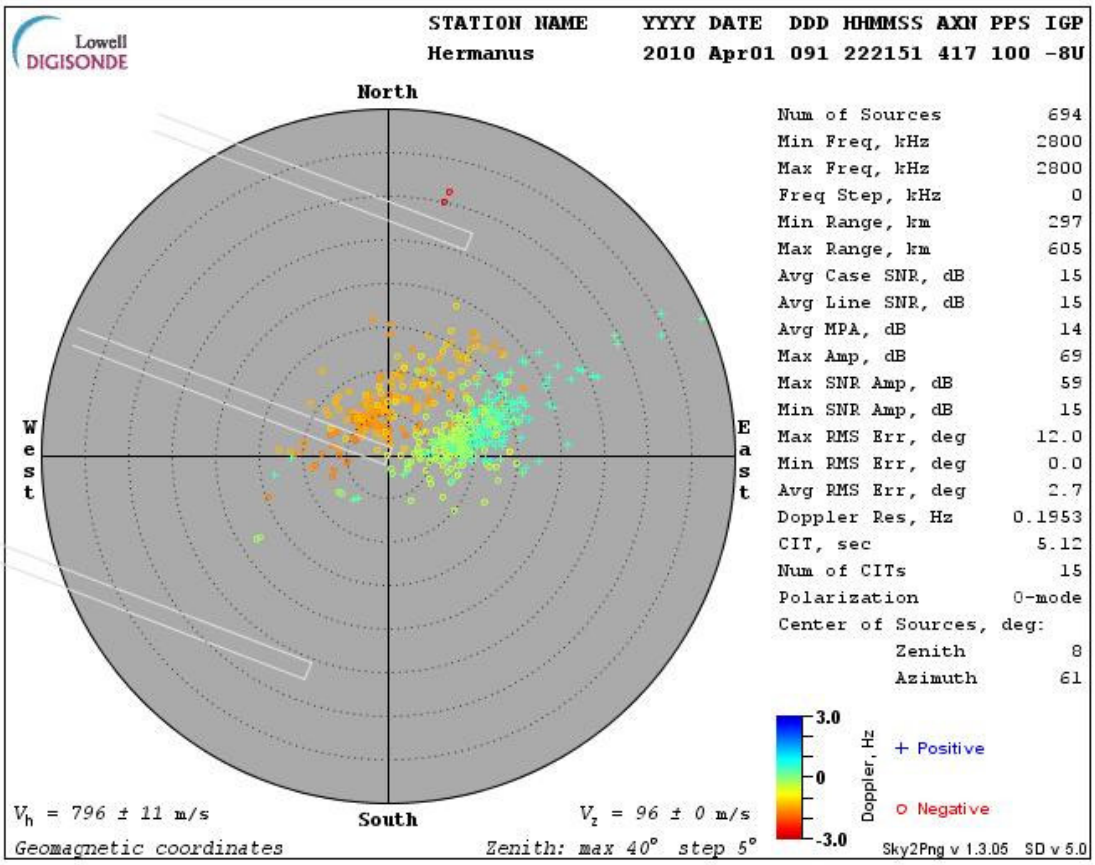

Figure 3.6: *Skymap produced by the DPS- 4D located at Hermanus Magnetic Observatory, South Africa.*

Looking at the above equations 3.1 and 3.2, there are three unknowns, V_x, V_y and V_z, which can be determined by measuring any three sources. However, there are always more than three sources and this makes the problem to be over determined. To solve this problem, the line of best fit is applied using the least squares method. This method is applied to all the Doppler measurements by minimizing equation 3.3 to find the solution to V_x, V_y and V_z, which gives the best estimate of the drift velocity (Reinisch et al., 2005).

$$\varepsilon^2 = \sum_i \left(\frac{2}{c} (\hat{k}_i . \overrightarrow{V}) f_R + \triangle f_i \right)^2 \tag{3.3}$$

Figure 3.7 shows the velocities in the North (V_x), East (V_y) and V_z derived from the DFT files using the Drift Explorer software that uses the above method in the DPS-4D.

3.4.1.3 Ionospheric tilt

In addition to drift velocities, sources can be used to estimate the local tilt of the ionosphere. This is done by calculating the offset of the "gravity centre" of skymap sources from the nadir. To improve the accuracy of the ray tracing application, the phase angles from the four antenna signals are used to obtain the 3D plasma distribution in the area surrounding the station (Reinisch, 2009).

3.4.2 Passive RF sensing mode

This mode of operation is used when the DPS-4D is used to monitor transmitters of opportunity within a defined radius. The signals received from the other transmitters are used to describe the characteristics of the ionospheric channel they have travelled through by looking at their phase delays. In most cases, this method is used when determining small-

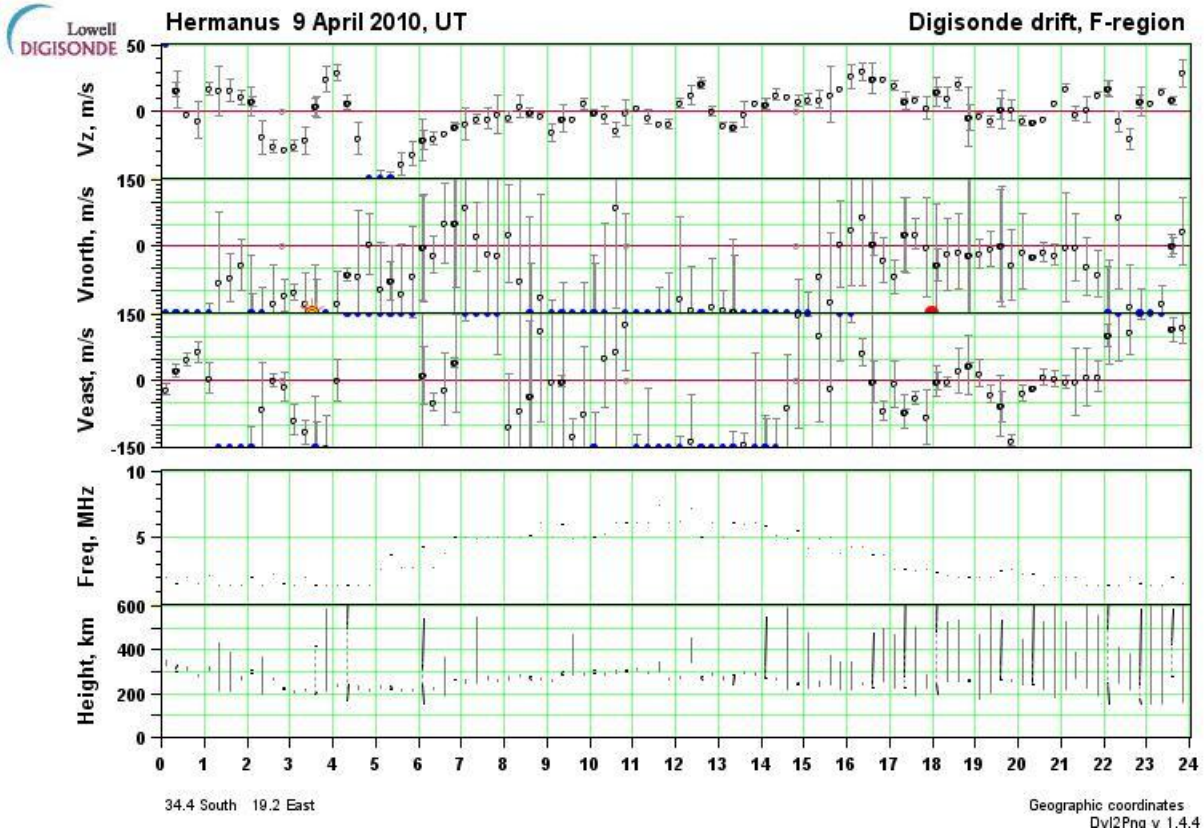

Figure 3.7: *Calculated drift velocities from the skymap data, with the error bars showing the spread of the measurements. The lower subplots show the frequency at which sounding was performed and the height at which the sources were detected.*

scale ionospheric irregularities (Reinisch, 2009). Earlier Digisondes could not use this mode due to the high volumes of time domain data to be processed. However, the DPS-4D with its large bandwidth and modern embedded computers has made this possible.

3.5 Summary

The parameters used in programmes for the DPS-4D were discussed, with emphasis on parameters used in drift mode sounding, as used for the experiment described in this thesis. Other possible DPS-4D measurements also received attention.

Chapter 4

Pc3 pulsations

4.1 Introduction

The Earth's magnetosphere is highly structured, in terms of both magnetic field and plasma characteristics. This structure influences the propagation of ultra-low-frequency (ULF) waves between the magnetosphere and the ionosphere. These waves lie in the frequency range of 1 mHz to 1 Hz and serve as a useful diagnostic tool for charaterising the magnetosphere. This chapter discusses the propagation of ULF waves from the magnetosphere to the ionosphere, the properties of ULF waves in the range of 20-50 mHz (Pc3 pulsations) and the way they are observed from the ground using different instruments. The information in this chapter will be used for setting up the experiment described in this thesis.

4.2 Propagation of ULF waves

Geomagnetic ULF oscillations are in most cases excited by a process involving the large wind shear between the high-velocity solar wind and the static magnetosphere. The waves may arise due to the Kelvin-Helmholtz instability and decay as they penetrate the magnetosphere. The mag-

netospheric plasma supports Alfvén waves and fast magnetosonic (FMS) waves. The produced perturbations in the Alfvén mode are guided by field lines and propagate with no distortions transverse to the field lines from the magnetospheric boundary to the boundary of the high latitude ionosphere. On the other hand, FSM waves propagate in any direction and generate compression and rarefication in both the magnetic field and plasma. The mode of propagation of these waves from the magnetosphere to the ionosphere depends on the Alfvén velocity, C_A

$$C_A = B_0/(\rho)^{1/2} \tag{4.1}$$

where B_0 is the magnitude of the geomagnetic field and ρ_0 is the density of the cold plasma (Alperovich and Fedorov, 2007).

This C_A is inhomogeneous, since both the geomagnetic field and magnetospheric plasma are also inhomogeneous. This inhomogeneity leads to the coupling of FMS and Alfvén waves which is mostly seen in regions of resonance (Chen and Hasegawa, 1974).

When the FMS wave encounters gradients (inhomogeneities) on its way these cause a guided Alfvén wave, which then propagates along the field lines to the ionosphere. These waves can penetrate the ionosphere to reach the ground but can also be partially reflected. If the double travel time between the ends of the field line coincides with the excitation period of an external source or one of the harmonics, the wave is resonantly amplified. This kind of resonance is known as field line resonance (FLR) (Walker, 2005).

If the amplified waves are Alfvén, they are associated with a longitudinal current when they propagate through the ionosphere. This current

does not penetrate the atmosphere, because of its insignificant conductivity but spreads over the ionosphere. However, if the incident waves are FMS-mode, the ionosphere appears to be transparent causing two types of currents - ionospheric and terrestrial. Pulsations due to these waves are in most cases global with certain simultaneous oscillations having been traced with confidence halfway across the globe, i.e., oscillations observed in one hemisphere are often observed in the opposite hemisphere (Alperovich and Fedorov, 2007).

Thus, there are two ways for FMS waves to reach the Earth:

- The re-radiation of a decayed FSM wave into an Alfvén wave guided along a Field line
- when the FSM wave is excited by a source located on the magnetospheric boundary and reaches the ground directly.

4.2.1 Classification of ULF waves

In 1958 the International Association of Geomagnetism and Aeronomy (IAGA) set up a four-person working group to reduce the proliferation of the newly recognized species of geomagnetic micro-pulsations. This group suggested and classified these pulsations based on whether they were continuous or irregular, which were then denoted as Pc and Pi respectively. These classifications were further broken into sub-classes depending on their predominant frequency or period as expressed in table 4.1 (Jacobs et al., 1964), where the integer following the prefix denotes the frequency

Table 4.1: Classification of pulsations by IAGA.

Notation	Period range (s)	Frequency (mHz)
Continuous		
Pc1	0.2 - 5	5000 - 200
Pc2	5 - 10	200 - 100
Pc3	10 - 45	100 - 22.2
Pc4	45 - 150	22.2 - 6.7
Pc5	150 - 600	6.7 - 1.67
Irregular		
Pi1	1 - 40	1000 - 25
Pi2	40 - 150	25 - 6.7

band. Since then, substantial effort has been put into understanding the generation, propagation and existence of these micro-pulsations.

4.3 Pc3 pulsations

Pc3 geomagnetic pulsations are quasi-sinusoidal variations in the Earth's magnetic field in the period range 10-45 seconds (Table 4.1). Their characteristics are consistent with those expected of transverse standing Alfvén waves along the geomagnetic field lines. Thus, their study is of importance because they provide us with information on how waves are generated both inside and outside the magnetosphere.

The energy of Pc3 waves is believed to be derived from two sources. The dominant source is the proton cyclotron instability in the solar wind. The other energy-generating mechanism is the Kelvin-Helmholtz instability at the magnetopause (section 4.2). The waves produced due to the latter excite field line resonance oscillations in the magnetosphere and are observed as Pc3 pulsations at higher latitudes. Pc3 pulsations that are observed in the middle and low latitudes are upstream waves generated due to ion-cyclotron instability by protons reflected off the bow shock along

the interplanetary magnetic field (IMF) lines. These are transmitted as compressional waves and propagate across the ambient field up to the inner plasmasphere to couple with various hydromagnetic (HM) oscillations which are later observed as magnetic pulsations.

Because of the spiral orientation of the IMF and the frequency dependence of Pc3 waves on the IMF strength, these waves are observed in the morning side with maximum power near 10:30 - 11:00 MLT which increases with the decreasing IMF cone angle (θ_{Bx}) (Engebretson et al., 1986). Measurements made by the synchronous satellite GOES2 (L = 6.67) also suggest that the frequency (f) of the pulsations in the Pc3 band increases with increasing IMF magnitude (Alperovich and Fedorov, 2007). An empirical relationship between f, B_{IMF} and θ_{Bx} was defined by Takahashi et al. (1984) namely

$$f(mHz) \approx 7.6 \times B_{IMF}(nT) \times \cos^2 \theta_{Bx}$$

Previously Pc3 pulsations were thought to be confined to middle and high latitudes, but these waves can be observed on the ground or in space at all magnetic latitudes. At high latitude the Pc3 pulsations comprise two principal components;

- A band-limited enhancement ("signal") usually centered around 20-30 mHz.
- Power law background "noise" with spectral density αf^{-p} where $p \backsimeq 3 - 4$ (Ponomarenko et al., 2005).

A recent study of these waves at low latitudes found that their occurrence probability is dominant when the solar wind velocity is in the range

of 400-700 km/s. Also, results obtained using data from the Image magnetometer array located in northern Scandinavia and the Arctic, show that the apparent phase velocity of Pc3 pulsations is directly poleward and rarely exceeds 100 km/s (Howard and Menk, 2005).

In relation to magnetic activity, Pc3 periods tend to decrease with the increasing K_p index. This is related to the inward movement of the magnetopause and plasmapause during higher magnetic activity (Gupta and Stening, 1971).

4.4 Observations of Pc3 pulsations

Observation of ULF pulsations started with Stewart (1861). He noted pulsations in a large geomagnetic storm recorded at Kew Observatory (51°29'N, 0°17'W). Later on, other observations were recorded by Angenheister in 1920, Rolf in 1931 and Sucks Dorff in 1939 who studied features of large amplitude, high monochromatic pulsations with frequencies between 10 - 20 mHz. Since then various steps have been taken towards observing these pulsations both on the ground and in space using instruments such as magnetometers and radar systems.

4.4.1 Magnetometer observation of pulsations

On the ground pulsations can be detected by using different types of magnetometer arrays. The application of magnetometers has proven to be one of the most successful methods of studying the spatial structure of hydromagnetic waves in the Earth's magnetosphere. There are different types of magnetometers and these include: magnetic variometers, proton precession magnetometers, fluxgate magnetometers, rubidium magnetometers and induction coil magnetometers. These detect pulsations

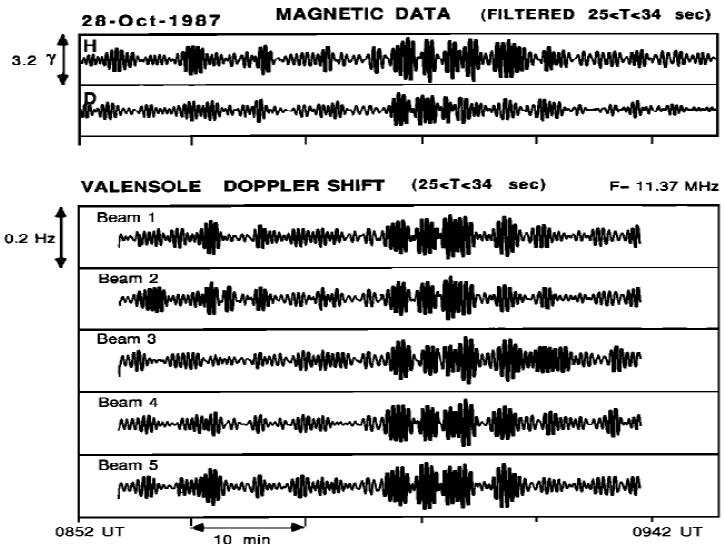

Figure 4.1: *Filtered Pc3 pulsations recorded on the ground using magnetometers and radar. The upper trace shows the H and D component recorded at Auray (47°40´N 2°58´W) October 28, 1987. The lower five traces show the radar Doppler shift variations recorded by the radar at Valensole (44°N, 6°E) operating at a sounding frequency of 11.37 MHz.*

by measuring perturbations in the north-south (H) and east-west (D) components of the Earth's magnetic field. These perturbations arise from the integrated effects of currents in the ionosphere. Furthermore, in the Pc3 range, the data recorded by these magnetometers ranges from a magnitude of 0.1 nT (nano Tesla) to 1 nT with periods that could run from 10 s to 45 s. The upper trace in figure 4.1 shows an example of Pc3 magnetometer data recorded at a mid-latitude station operated at Auray (47°40´N 2°58´W, October 28, 1987) near the coast of Brittany and filtered between 25 s and 34 s (Bourdillon and Delloue, 1989).

4.4.2 Radar observation of pulsations

The ability to detect Pc3 pulsations over a large field of view came with the use of radars which detect pulsation signatures by measuring ionospheric Doppler changes and the polarization of radio waves. The

Doppler changes can be caused by Alfvén waves which relate to electron transfer along the external field or pressure of the FMS waves, causing perturbations in the plasma density. In the F region where Pc3's are mostly observed, the plasma drifts under the influence of the electric field ($\overrightarrow{E}$) of the MHD wave at a velocity of

$$\overrightarrow{V} = (\overrightarrow{E} \times \overrightarrow{B})/ \mid B \mid^2$$

In a Cartesian coordinate system (x, y, z) the magnetic field $\overrightarrow{B}$ is inclined at an angle$I$ in the (x, z) plane and the vertical component of the electron drift is

$$V_{ez} = -(Ey/B)cosI$$

It's this V_{ez} that causes the Doppler shift in the frequency of radio waves from radars as shown in the lower five traces in figure 4.1 recorded at Valensole (44°N, 6°E).

The use of the radar network technique to observe pulsations was first seen in the Scandinavian twin aurora radar experiment (STARE). Radio waves were used to observe Pc5 pulsations with a spatial resolution of 20 km over a 200,000 km² grid. Due to this experiment, Walker et al. (1979) were able to show that Fourier amplitudes and the phase of the spectral peaks of oscillation depend on the latitude. However, STARE type radar networks cannot be used to detect periodic Pc3 pulsations, because the electric field intensity was below the threshold field required to drive the irregularities.

Results from the STARE VHF radar stimulated the development of an improved radar net-work known as the Super Dual Auroral Radar Network (SuperDARN). It was developed primarily for large-scale studies

on ionospheric convections over higher latitudes (Greenwald et al., 1995). This radar network overcame STARE limitations by operating at HF and exploiting ionospheric refractions (i.e. the HF signals are reflected from the F-region which does not require the existence of a background electric field). The network consists of 16 radars with overlapping fields of view (FOV). Ten of these radars are operated in the northern hemisphere and six in the southern hemisphere with one of them, known as the SHARE (Southern Hemisphere Auroral Radar Experiment) located at the SANAE (South African National Antarctic Expedition) base.

Pc3 pulsations have been studied by SuperDARN by modifying the radar scanning sequence such that increased temporal resolution is available over a restricted spatial area. Some of the research on Pc3 pulsations using this network has been reported by (Ponomarenko et al., 2005). They suggested that the compressed Pc3–4 waves produced in the upstream solar wind travel earthward from the magnetopause in the magnetic equatorial plane depositing energy into the Alfvénic modes. They do this as either forced or third harmonic FLR's that reach ionospheric heights along magnetic field lines.

In addition to the SuperDARN and STARE networks, a new sounder known as the Doppler Pulsation Experiment (DOPE) has been employed to study ionospheric changes. This sounder is an HF radar system which offers the advantage of being able to select the vertical height when sounding (by changing the sounding frequency), as well as having a high spatial and temporal resolution. The spatial resolution in Doppler sounders is determined by the area over which integration of data takes place. In

most cases, this turns out to be the area of the Fresnel zone with a radius (R) given by

$$R = \sqrt{r_0 \lambda} \tag{4.2}$$

where r_0 is the height of reflection and λ is the free space wavelength (Wright et al., 1997).

This kind of sounder has been used in Leicester, United Kingdom, since 1995 and has proved to be a success in the observation of Pc3-4 and Pi 2 pulsations.

4.4.3 Observation of Pc3 pulsations in South Africa

The study of pulsations in South Africa has been ongoing since 1987, with the Hermanus Magnetic Observatory being one of the main research centres. Being a low latitude station, most of the ULF waves observed at HMO are Pc3 pulsations. The frequency of oscillation of the waves at this station is mainly in the range 20-100 mHz with typical amplitudes ranging from 0.1-1.0 nT (Sutcliffe et al., 2002).

The study of Pc3 pulsations using sounders (radar) was first done as a collaborative effort between the HMO and the Department of Physics at Rhodes University in Grahamstown, South Africa. This work involved the use of data recorded (November 1983) by a digital chirp ionosonde (located at Grahamstown 33°2 S, 26°50 E and L=1.83) and digital induction magnetometers (located at Hermanus 34° 43E S, 19°23 E and L=1.85) which recorded the simultaneous Pc3 components in the north-south (H) and east-west (D) on the ground. In this research the oscillations of ionospheric Doppler velocity were associated with Pc3 geomagnetic pulsations recorded at ground level (Sutcliffe and Poole, 1984). To understand the mechanism by which Pc3 pulsations contribute to the Doppler shift, Sut-

cliffe and Poole (1989) presented a model in which they identified three mechanisms: a "magnetic" mechanism, an "advection" mechanism and a "compression" mechanism. The "magnetic" mechanism accounts for changes in the refractive index due to changes in the magnetic field intensity requiring no bodily movement of electrons. The "advection" mechanism describes a change in refractive index due to a vertical bulk motion of electrons in the ionosphere. This vertical motion is the vertical component of the $\overrightarrow{E} \times \overrightarrow{B}$ plasma drift velocity which arises due to the fact that the oscillating magnetic field lines are not completely orthogonal to the ground. The "compression" term relates to changes in the refractive index brought about due to changes in the local plasma density caused by propagation in the E-region of a compressional fast mode wave associated with the initial incident Alfvén wave (Jacobs et al., 1964).

The research by Sutcliffe and Poole, (1984, 1989) inspired a number of research activities to understand Pc3 pulsations over South Africa and around the world using radars and ground magnetometers. However, the use of radar networks to observe pulsations has mostly been confined to auroral, cusp and polar cap regions due to the difficulty of identifying them in other areas. Some of the difficulties include: the three-dimensional nature of the data (time, range and beam), the presence of fast background drifts with velocities greater than 500 m/s which obscure ULF wave signatures with low velocities and the presence of multiple propagation modes.

Although all these difficulties do exist, there is still a large number of unknown features about the Southern African ionosphere which need to be studied. One of these features is the use of the ULF pulsations as a diagnostic tool for probing the magnetosphere. But, as stated above, at low

latitudes such as Hermanus the most commonly observed pulsations are daytime Pc3's. For this reason, the experiment at the HMO to expand the capabilities of the new state-of-the-art Digisonde (DPS-4D) concentrated on the search for Pc3 pulsations.

4.5 Summary

In this chapter the propagation of ULF waves from the magnetosphere to the ionosphere and the ground as FMS waves or Alfvén waves was discussed. The properties of ULF waves in the Pc3 band and their detection using magnetometers and radars has also been discussed. The next chapter describes an experiment attempted at HMO the aim of which was to observe Pc3 pulsations using the DPS-4D which is a sophisticated HF radar system developed for other purposes.

Chapter 5

Description of the experiment

5.1 Introduction

This chapter describes the experiment to investigate the capability of the DPS-4D to observe Pc3 pulsations. The DPS-4D used in the experiment is located at the mid latitude station, Hermanus (34.4°S, 19.2°E), South Africa, with station ID 934 and URSI code HE13N. The station ID is a 3 digit number that is used to label all data products and the URSI code is unique 5-character code assigned by the International Union of Radio Science (URSI) to observatories based on the location of the sounder. This experiment was done from April to September 2010. The primary objective was investigate the possibility of using the DPS-4D to observe Pc3 pulsations.

5.2 Experiment setup and overview

The setup of this experiment involved the optimization of different parameters in the DCART software to form a program to be run on the DPS-4D as well as simultaneously recording magnetometer data. The magnetometer data was compared to ionospheric data. Depending on the

relationship obtained from the two data sets, a conclusion was drawn on the ability of the DPS-4D to observe Pc3 pulsations.

5.2.1 Optimization of parameters

To optimise the parameters used on the DPS-4D, the following Pc3 pulsation properties were considered:

- The period of Pc3 pulsations at low latitudes range from 20 s to 45 s (Jacobs et al., 1964).
- An event of Pc3 pulsations can exist for more than an hour (Gupta and Stening, 1971).
- Pc3's are most likely to be observed at the critical frequency of the F-region, given that irregularities near the reflection height have the greatest effect on phase path changes (Marshall and Menk, 1999).
- In the low and mid-latitudes, Pc3 pulsations are daytime events (Marshall and Menk, 1999).
- The Doppler shift of Pc3 is defined in the range $7 < f < 50$ mHz. Marshall and Menk 1999.

The above properties were used to determine the values of the parameters in table 5.1 for the DCART. An explanation of the choice of these parameters follows.

To observe Pc3 pulsations in the ionosphere, a continuous observation of perturbations at a particular height of the F-region was done. This was achieved by setting FSL to "fixed frequency", which places the DPS-4D

Table 5.1: Optimised parameters for Pc3 observation.

Parameter	Set value	Parameter	Set value
FSL	fixed	WF	16-chip complementary wave
FF	5.4 MHz	Pol	O-only
FFR	15	FPS	Doppler calculation
NFS	none	RFIM	checked
SR	80 km	CEQ	checked
NS	512	DRW	150 - 800 km
IPP	10 ms	NBR	4
NIR	128	OPF	DFT
IPS	enable	SPF	checked
CG	full gain 50 dB	SPRF	not checked
AGC	use existing gain table	FO	checked
RxG	+30 dB	FFS	none

in the drift mode. To increase the number of data points per observed height, the FFR was set to a maximum value of 15 times.

Since Pc3 pulsations can best be detected near the F-layer critical frequency, the FF value was set just below the average of the recently calculated foF2 value. This was done by enabling the frequency override (FO) parameter which shifts the fixed frequency up and down to target the F-region by using data from the recent ionogram (as discussed in chapter 3). For ionogram processing, the maximum zenith of vertical echoes was set to 20° and maximum eligible zenith angle for directions was set to 45°. The phase difference minimization analysis (as discussed in chapter 2) was used for direction finding.

If the period of Pc3 pulsations is Tpc3 as shown in figure 5.1, the CIT value needed has to be smaller than $\frac{\text{Tpc3}}{2}$, in order to increase the number of data points over the sampling period and to prevent aliasing. However, the smaller the CIT, the less the averaging of the Pc3 Doppler shift. Therefore, a small CIT value that would be able to resolve enough

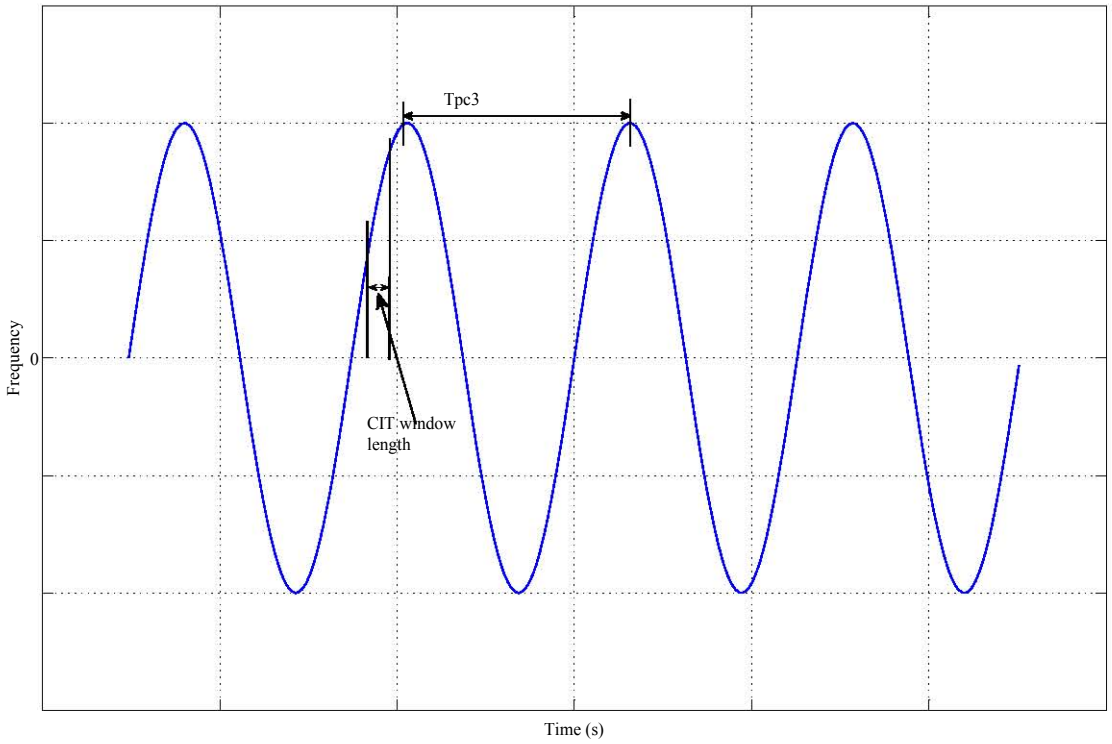

Figure 5.1: *Averaging of a CIT window over a pulsation period.*

data points and also provide a reasonable resolution was chosen with many repetitions. The parameters used to obtain this CIT were NS = 512, IPP = 10 ms, NIR = 128 and Pol = O-only, and it was calculated as follows:

$$CIT = 2 * IPP * NIR$$

$$= 2.56 \text{ s}$$

The need for this small CIT value ruled out the possibility of using frequency multiplexing which is often used to increase the CIT value (i.e. high Doppler resolution) in the drift sounding mode. Thus, the setting NFS was set to "none", as shown in table 5.1.

Although a better CIT value would have been obtained by manually setting the IPP to a desired value, the DCART software does not allow this. In fact, the manually set values reset to 10 ms during sounding. With this limited IPP, the maximum number of pulses per second (frequency) that could be obtained was 100 Hz.

128 was chosen as the NIR value, because the output file format (DFT) can only take a maximum of 128 Doppler spectral lines.

To avoid the absorption region (D-region), the SR was set to 80 km. Beyond the SR height, the NS parameter to be averaged for each transmitted pulse was set at 512.

As far as the system settings are concerned, CG was set to a full gain of 50 dB, AGC was set to use the existing gain table, and the waveform for sounding was set to 16-chip complementary code.

Finally, a Doppler calculation was chosen with a 1/2 Doppler shift enabled. The 1/2 Doppler shift would assist in determining whether the

small Doppler shifts were up or down (as discussed in chapter 2). The RFIM and IPS techniques were enabled to reduce the amount of noise and suppress interferers with the maximum number of RFIM iterations set to 15. Since data from one polarisation can be used to provide full information about the pulsations (Marshall and Menk, 1999), and to reduce the size of the data to be stored, only the O-wave was chosen for detection and the number of best ranges (NBR) around the strongest echo set to 4. These NBR was selected from the data windowed to run from 150 km to 800 km(set to cover the E and F regions).

The final results were saved in the DFT file format and analyzed after the sounding had been complete.

5.2.2 Programme campaigns

When all the parameters in the DCART software had been set, the obtained programme had a running time of 38.430 s. This programme was scheduled to run during the day (between 5:00:00-19:00:00 local time) since at low latitudes, such as at the HMO, Pc3 pulsations are daytime events.

The first run of the designed programme produced one DFT data file every 15 minutes, because it had to slot into the regular DPS-4D programme schedule. From a single DFT file produced, a snapshot of only 38 seconds of observations could be obtained. On average this snapshot provided information for one and one half periods of a pulsation data recording. To increase the observation time, a balance between the running time of the Pc3 programme and the other programmes on the DPS-4D was found. This gave the Pc3 pulsation program a chance to run repeatedly 8 times (using the ASAP option) after every 11 minutes when

all the other measurements had been done. This process increased the time of observation for a single snap shot from 38 s to approximately 307 s (8×38.430 s).

5.2.3 The magnetometer

The magnetometer used in this experiment is an induction coil magnetometer located at the HMO (34.4°S, 19.2°E). It consists of 2 m long mu-metal rods (sensors) with 100000 turns of copper wire. They are aligned with the geomagnetic north-south, east-west and vertical directions to give the H, D and Z components. The variations detected by these sensors are passed through an amplifier connected to a GPS module for the time stamp. The raw data collected over time from these sensors is sampled at one second with a resolution of 0.1 nT.

5.3 Data analysis and discussion

5.3.1 Active Pc3's timestamp spotting using magnetometer data

After sounding was done and a number of DFT files stored, finding the time stamps for the active Pc3's from the many files proved to be a challenge. Thus, data from magnetometers were used as a sorting tool for the files that were expected to contain active Pc3 pulsations. This sorting process was performed based on the fact that the propagation of ULF waves down through the ionosphere causes oscillations which lead to Doppler shift in the HF radio transmissions. There is a high correlation between these Doppler shifts and the magnetic pulsations recorded on the ground (Marshall and Menk, 1999).

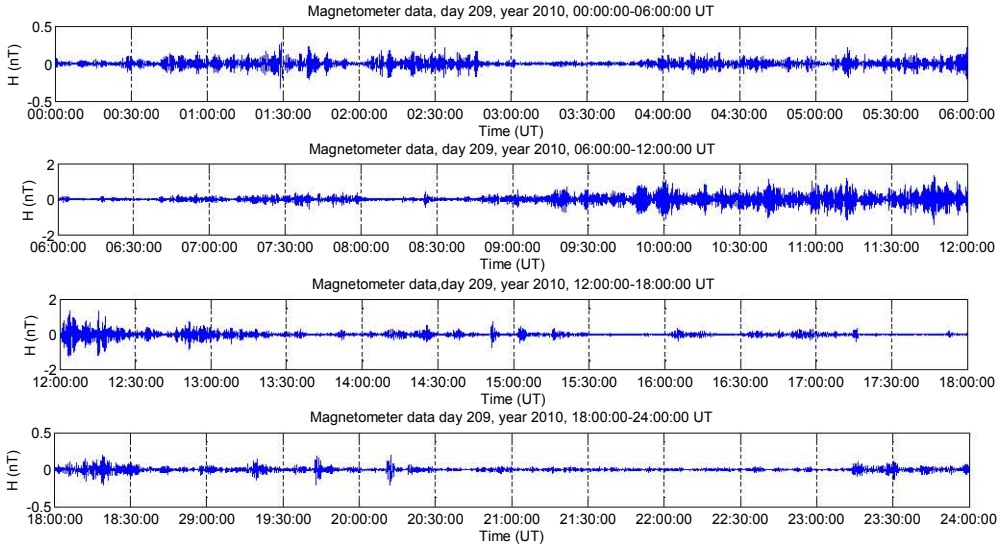

Figure 5.2: *Magnetometer data for day 209 year 2010 bandpass- filtered within the Pc3 band (2-50 mHz).*

5.3.2 Magnetometer data analysis

The raw data obtained for each day from the H and D components of the magnetic field was split into six-hourly intervals. This data was band pass-filtered in the frequency range 2 - 50 mHz using a Butterworth filter. Figure 5.2 shows an example for day 209 year 2010, filtered and split into six hourly intervals.

To determine the possibility of any pulsations in the Pc3 frequency band, the filtered data was transformed into the frequency domain with the purpose of looking at its spectral representation as shown in figure 5.3. These plots clearly show a high spectral spike at about 44.59 mHz between 06:00:00-12:00:00 which lies in the Pc3 band.

To expand the view of what happens within the identified interval, data was split further using a window of 300 seconds. This helped to determine the time stamp when the pulsations were visible and contained

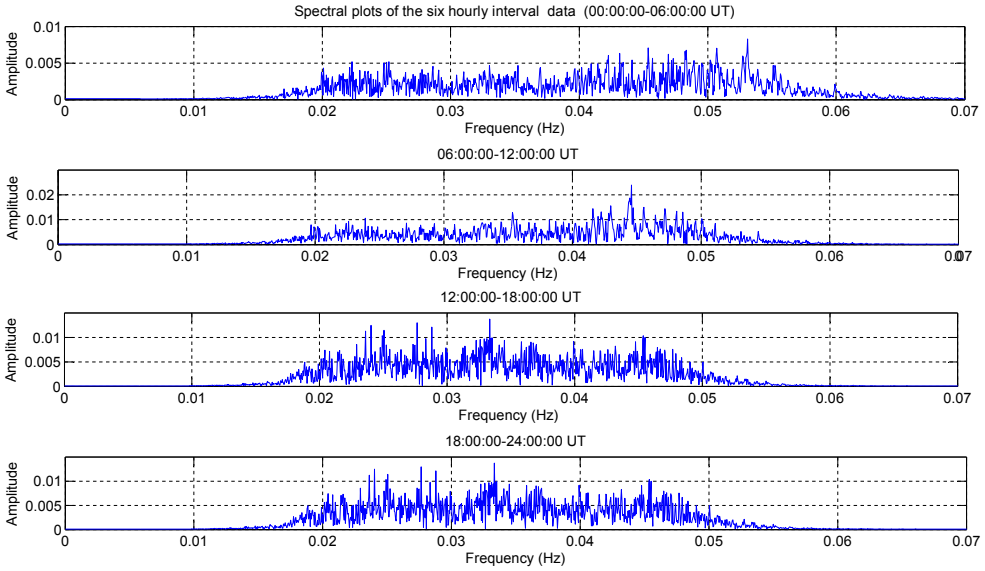

Figure 5.3: *Spectral plot for the six-hourly interval-filtered magnetometer data. The second trace shows a dominant frequency at 44.59 mHz which lies in the Pc3 band.*

high amplitudes. Figure 5.4 shows an example of such a window running from 11:05:00 to 11:10:00 UT for day 209 of 2010. The pulsations in this window have periods of approximately 20 s and a maximum peak-to-peak amplitude of 1 nT.

After magnetometer data analysis the two days that showed the strongest pulsation amplitudes were chosen for this thesis, namely day 209 and 236 of the year 2010.

Using the identified time stamps when the pulsations were active in the magnetometer data, the DFT files that corresponded to these times were extracted from the files and stored for further analysis. However, there were times when the magnetometer recording showed high amplitudes, but the DFT files did not exist. This was due to the limitation of the DPS-4D mentioned earlier, namely that it has to perform other tasks during the running of the experiment. Figure 5.5 shows a plot of the

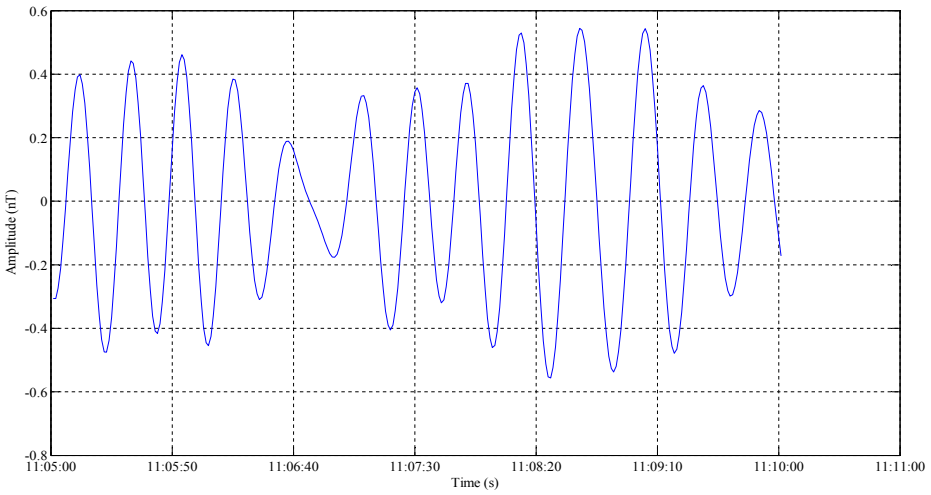

Figure 5.4: *300 seconds of pulsation data running from 11:05:00-11:10:00 UT of day 209, 2010. The period of these pulsations is 20 s with a maximum peak-to-peak amplitude of approximately 1 nT.*

filtered magnetometer recordings between 06:00:00-12:00:00 UT of day 209 of 2010, with the red pillars showing the times when DPS-4D did measurements for the experiment within this interval. Each red pillar is equivalent to 307 s (≈5 min) of continuous sounding.

5.3.3 Data extraction from DFT files

In each DFT file there was data for each of the four receiver antennas. But since the data from all four antennas is presumed to be from the same height, data from only one antenna was chosen arbitrarily for analysis. For this experiment, data from antenna one was chosen.

The data comprised 4 heights each having 15 spectra. Each of the spectra contained 128 amplitude values with their corresponding phase values (Refer to chapter 3 for DFT file format). Using the Drift Explorer software for analyzing DFT files, the height with the best echo amplitudes

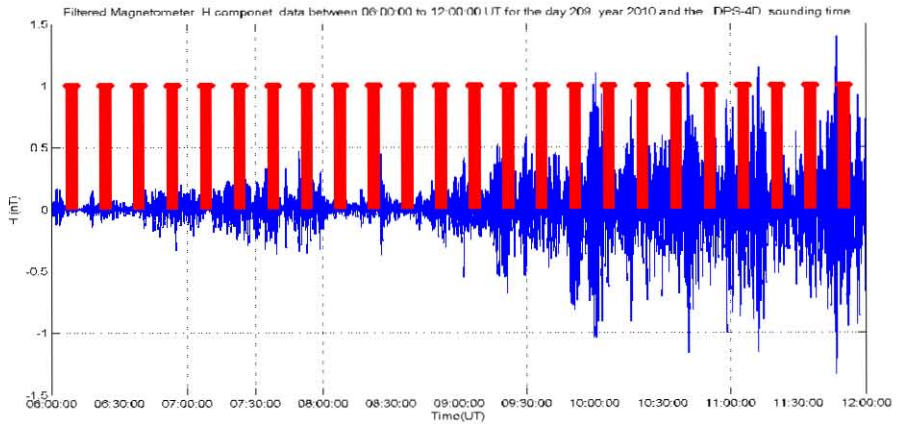

Figure 5.5: *Filtered H component of magnetometer data between 06:00:00 to 12:00:00 UT together with the DPS-4D sounding times (red pillars) for the experiment.*

was chosen from the 4 recorded heights. For example, figure 5.6 shows a waterfall representation of 4 ranges (280 km, 282 km, 285 km, 287 km) using a linear scale from a DFT file generated at 11:55:20 UT on day 209 of 2010. Height 285 showed the best amplitude of 2818.38 as compared to the rest and was chosen for analysis.

Although this software plots out the spectra, the Doppler changes due to the pulsations were too small to be noticed in the drift spectrum plots. To observe these small changes, a short time Fourier Transform was applied to the time domain signal.

To transform back to the time domain, each of the 128 spectral amplitudes and phase values that corresponds to the chosen height were used to form a complex signal "Z_k" to which the inverse discrete Fourier transform was applied $(F_n(Z))$,

$$Z_k = A_k(\cos\phi_k + j\sin\phi_k)$$

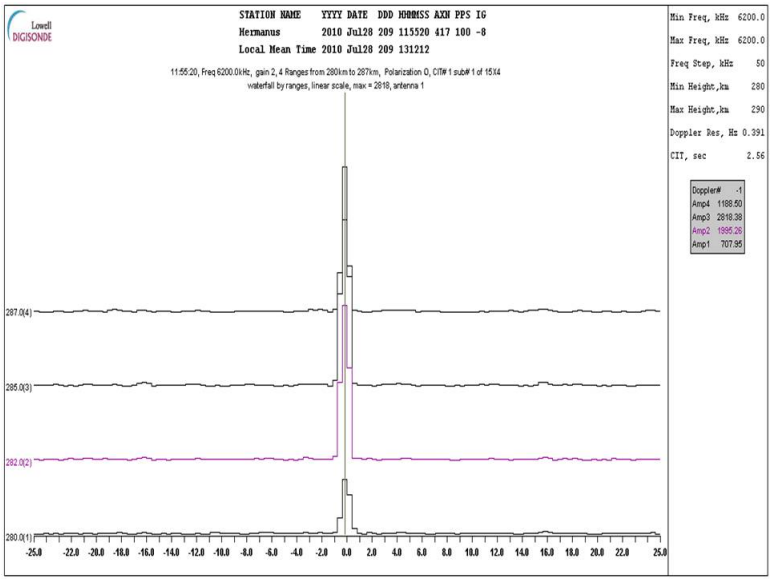

Figure 5.6: *Waterfall representation of raw data from a single DFT file generated at 11:55:20 UT on day 209, of 2010.*

$$= A_k \exp(j\phi_k) \tag{5.1}$$

$$k = 0, 1, 3, ..., N-1$$

$$F_n(Z) = \frac{1}{N}\sum_{k=0}^{N-1} Z_k \exp(\frac{j2\pi nk}{N}) \tag{5.2}$$

$$n = 0, 1, 3, ..., N-1 \tag{5.3}$$

where A_k and ϕ_k are the different spectral amplitudes and phase values respectively. Figure 5.7 shows the spectrum and phase of the first 128 data samples used to form the time domain signal.

The above process was done for all 120 spectra (from the 8 DFT files generated in one continuous sounding) within the chosen height and the

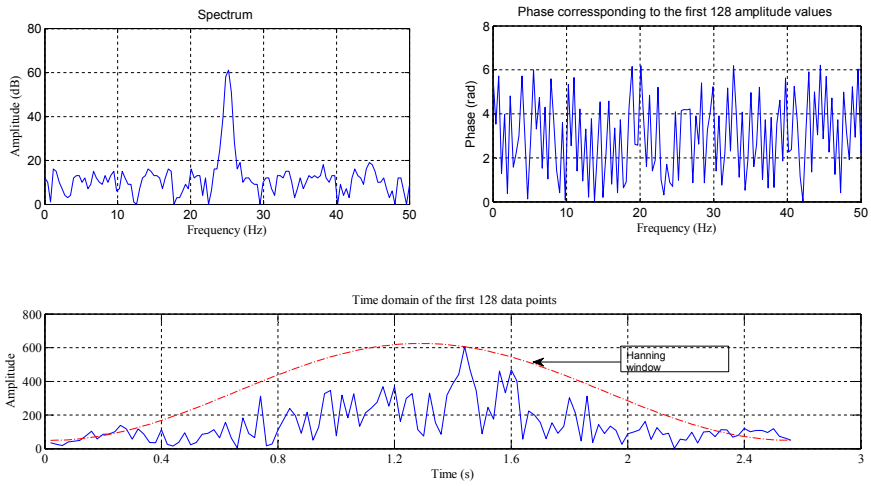

Figure 5.7: *Plot of the spectrum, phase and the time domain signal for the first 128 data samples from antenna #1 at height 285 km.*

data obtained concatenated to form one array consisting of 15360 data points.

In figure 5.7 it is clear to see that the Hanning window that was applied to the signal when transforming to the frequency domain was not removed after the inverse transform. This is because when applying the Hanning window, the data points at both ends of the signal smoothly approach zero. Removing the window would lead to some of the data points being divided by approximately zero. This would cause spurious spikes at the ends of the signal which would then shadow out the main signal. As a precaution, a Hanning window of 128 points was maintained throughout the analysis process.

5.3.4 Short Time Fourier Transform (STFT)

The Short Time Fourier Transform is the most widely used method to study non-stationary signals. It involves the process of using a window to break the time signal into segments which are then Fourier-analyzed. The smaller the segments, the more uncertain the frequencies that exist in that segment. Using this knowledge, it's easy to tell how the spectra vary with time.

Although this technique works well, meaningful results depend on how small the short duration signals are. This process of losing the information is due to the uncertainty principle as applied to these short term intervals. To illustrate how the STFT works, consider a signal $S(t)$ at time t, to be divided into small segments using a window $h(t)$. The small segment signal is then given by

$$S_g(\tau) = S(\tau)h(\tau - t) \tag{5.4}$$

where τ is the running time.

The window used in this process must act such that S_g is defined as

$$S_g \sim \begin{cases} S(\tau) & \text{for } \tau\text{near } t \\ 0 & \text{for } \tau\text{far away from } t \end{cases} \tag{5.5}$$

To find the distribution of the frequencies within this segment, the Fourier transform of S_g is taken to give the results in equation 5.6.

$$S_g(\omega) = \frac{1}{\sqrt{2\pi}} \int S_g(\tau) \exp(-j\omega\tau) d\tau \tag{5.6}$$

$$= \frac{1}{\sqrt{2\pi}} \int S(\tau)h(\tau - t) \exp(-j\omega\tau) d\tau$$

From the above result, the energy density spectrum (P_s) is

$$P_s = \mid S_g(\omega) \mid^2 = \mid \frac{1}{\sqrt{2\pi}} \int S(\tau) h(\tau - t) \exp(-j\omega\tau) d\tau \mid^2$$

In the case of a discrete signal $S(n)$ at the time n, its Fourier transform and power spectrum are given by

$$S(n, \omega) = \sum_{m=-\infty}^{\infty} S(m) w(n - m) \exp(-jm\omega) \tag{5.7}$$

$$P_s = \mid S(n, \omega) \mid^2 = \mid \sum_{m=-\infty}^{\infty} S(m) w(n - m) \exp(-jm\omega) \mid^2 \tag{5.8}$$

where m is the auto correlation lag and $w(n)$ is the window function.

To reduce the artifacts at the boundary, the short frames or segments are overlapped. This graphical display of the P_s is known as a spectrogram. Figure 5.8 shows a spectrogram for the data obtained between 09:51:30 and 09:56:37 UT for day 209 of 2010. The height chosen for analysis was 300 km and the sounding frequency was 4.9 MHz. The specifications for generation of the spectrogram included: a Hanning window of 128 points, 127 overlapping segments with a 50% overlap between the segments, sampling frequency of 50 Hz and 128 number of frequency points (NFFT). The NFFT affects the grid on which the spectrum is evaluated, but does not enhance the physical resolution. The higher the NFFT, the finer the axis grid. If one chooses a NFFT that is greater than the data segment, the Fourier transform is padded with zeros and all the data samples are applied to the transform. On the other hand, if the NFFT is less than the data segment, some data points are lost, hence poorer frequency resolution. However, in this case the NFFT value is limited to 128 points because of the Hanning window which could not be removed from the data. The sampling frequency used was based on the inter-pulse period

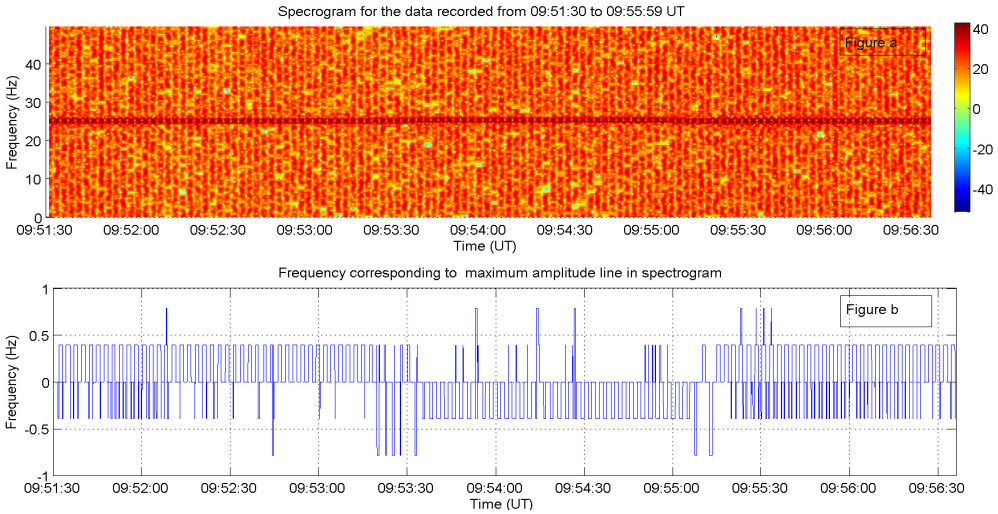

Figure 5.8: *a: Spectrogram for the timestamp 09:51:30-09:56:37 UT of day 209, of 2010 developed using the STFT. The dark red line centered at 25 Hz shows regions of high amplitude (120 spectra peaks). b: Frequency corresponding to the maximum amplitude line running across the spectrogram.*

of 10 ms for each complementary code, which turns out to be 20 ms (50 Hz) for the two codes that have to be sent to complete a transmission by the DPS-4D (as discussed in chapter 2).

In figure 5.8a regions of low amplitude can be seen along the high amplitude line that runs across the spectrogram centered at about 25 Hz. This is due to Hanning window of 128 points that was not removed from the inverse Fourier transformed data (as mentioned previously).

It was expected that the centre line would follow a sinusoidal trend should pulsations be observed (i.e. the frequency is expected to change with time due to the Doppler shift induced by the Pc3 pulsations). However, this was not the case.

Figure 5.9a illustrates what happens within the spectrogram. Assume that the pulsation driving the ionosphere has a maximum and a minimum velocity vmax and vmin respectively. When the velocity is zero, the

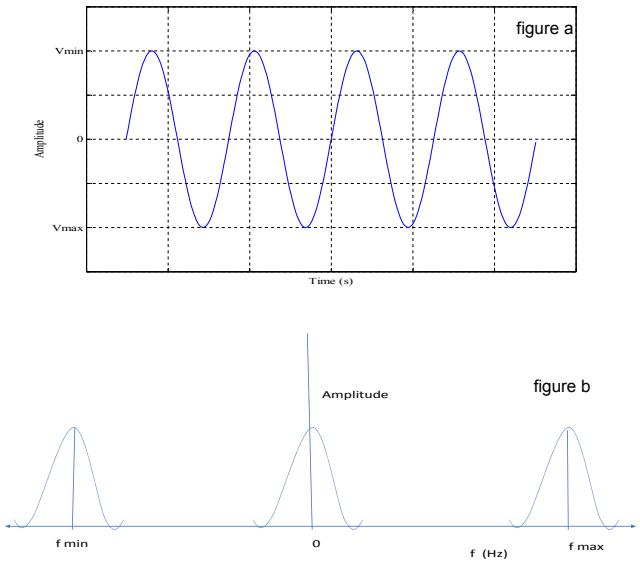

Figure 5.9: *a: Pulsation that could be driving the ionosphere, with maximum and minimum velocities vmax and vmin respectively. b: Spectrum changing position due to Doppler shift induced by the movement of the ionosphere.*

Doppler shift is constant due to the ionosphere being stationary. As the velocity increases from zero vmax, the Doppler shift is negative due to the ionosphere moving away from the observer. If the velocity decreases from 0 to vmin, the Doppler shift is positive due to the ionosphere moving towards the observer. Figure 5.9b shows how the generated spectra would change position in response to the motion of the ionosphere.

However, if the increase in velocity from zero to vmax or vmin is too small to be resolved by the DPS-4D, the motion of the ionosphere is recorded as being stationary with a constant Doppler shift. This is believed to be the case in figure 5.8b, where a single line of frequency corresponding to the maximum amplitude line in the spectrogram was

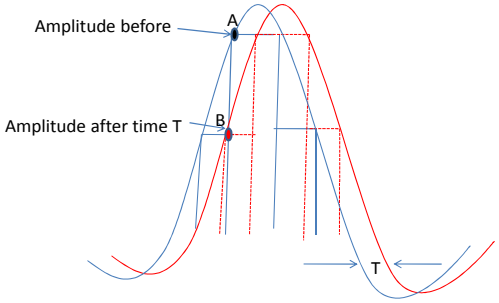

Figure 5.10: *Two spectra showing how a point changes amplitude from A to B after a sampling period T.*

extracted and plotted. It's noteworthy that not much information concerning Pc3 pulsations would be derived from this plot.

Since pulsations could not be resolved through the use of frequency, another analysis method was adopted. This method involves looking at how a single point of amplitude changes position with time during the observation period. Figure 5.10 demonstrates the expected. Assume that the spectrum shown in blue was generated before a time T (sampling period). If a point on this spectrogram with amplitude A is chosen, after a time T a new spectrum (shown in red) will be generated but shifted in time. In the latter case, the same point now exhibits a different and lower amplitude B. This change in amplitude, indicates whether the motion of the ionosphere was up or down depending on the motion induced by the pulsations. However, this method has limitations when the pulsations are not strong enough to cause a measurable shift in the spectrum.

To choose which line of amplitude to analyze, three lines (63, 64, 65) were extracted from the spectrogram. These lines were chosen because they represent the highest amplitudes for each single spectrum. Of the three, only the line with the best amplitude was chosen. Figure 5.11a

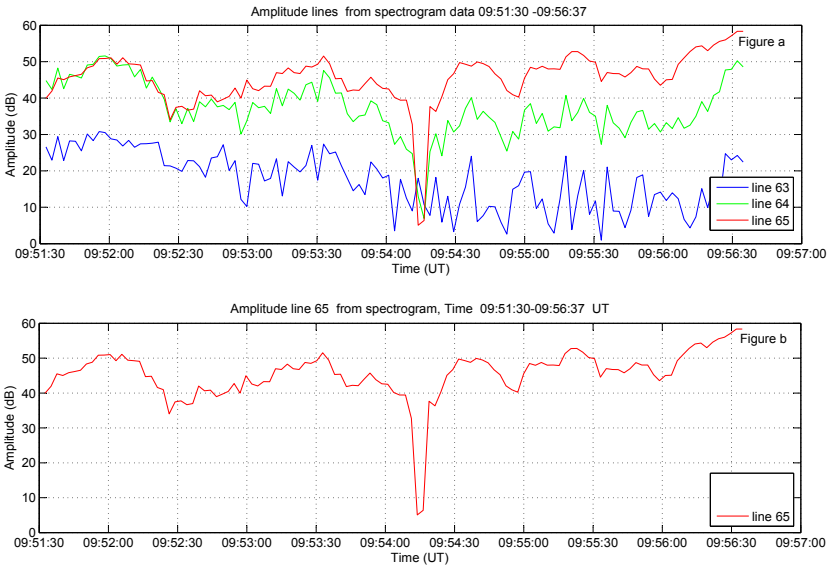

Figure 5.11: *a : Three amplitude lines (63, 64, 65) extracted from the spectrogram. b: Line 65 with the best amplitude among all the three lines of amplitude.*

shows the three extracted lines from the data recorded from 09:51:30 to 09:56:37 UT on day 209 of 2010. Line 65 (Figure 5.11b) shows dominance in amplitude and was chosen for analysis.

In figure 5.11b the extracted line shows a sinusoidal shape in some regions, but is not consistent. To smooth the shape, a linear smoothing function known as Lowess was applied to the extracted data. This smoothing procedure pays more attention to the local points round the value to be smoothed, such that if y is the smoothed value corresponding to data point x_i, it is obtained on the basis of the data points around it within a band of a certain width. The point x_i is the midpoint of the band and it gets the highest weight. The weights for the other data points decline with their distance from x_i according to weight function. The weighted least squares method is used to find the fitted value corresponding to x and then taken as the smoothed value. This procedure

is repeated to obtain the remaining smoothed values. This means that a separate weighted regression is estimated for every point in the data (Cleveland, 1979; Royston, 1992).

After the data was smoothed, a smooth spline curve was fitted onto the new data as shown in figure 5.12a. The generated curve was then plotted alongside the corresponding H-component of the magnetometer data (Figure 5.12b) to find any correlation between the two. However, no correlation was found. Based on the study by Marshall and Menk (1999) which found that ground-ionosphere correlation coefficients are slightly higher when evaluated using the magnetometer D component than for the H component, the D component of the magnetometer data was also plotted (figure 5.12c). Compared to the H component, the D component was found to exhibit amplitudes that were less than 0.3 nT. These low amplitudes were thought to be the cause of the inability to observe Pc3 pulsations in the DPS-4D data.

As an additional analysis, DPS-4D data recordings that corresponded to magnetometer data with higher amplitudes (1.2 nT peak to peak) and better correlation between the H and D components were chosen for analysis for the time stamp 07:51:30-07:56:37 UT, on day 236 of 2010, as shown in figure 5.13. The sounding frequency of the DPS-4D during this time was 3.7 MHz and the range chosen for analysis was 235 km. However, even with the high amplitudes and the high correlation between the H and D magnetometer data sets (figure 5.13c and b), still no sign of pulsations or correlation could detected in the DFT recordings (figure 5.13a) and the magnetometer data. This inability to detect Pc3 pulsations in the DPS-4D data may be related to the resolution not being high enough and the

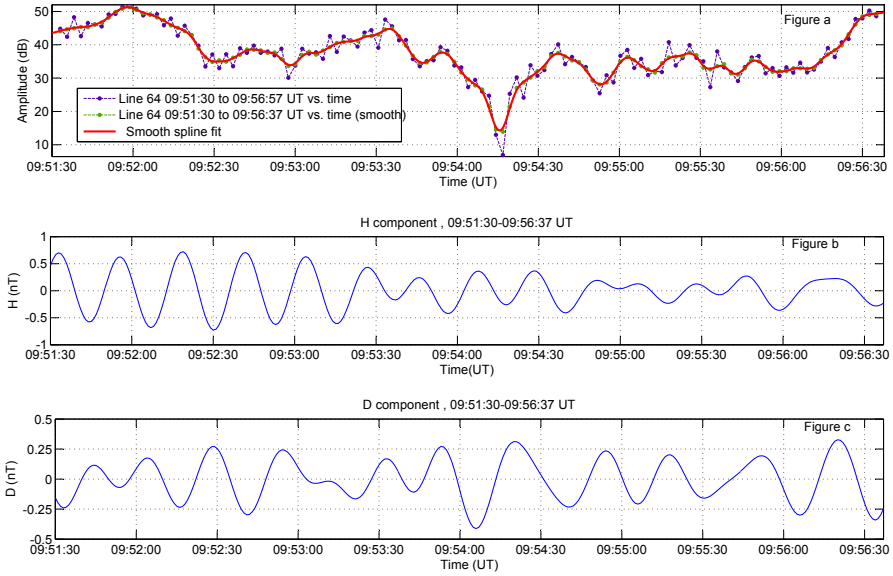

Figure 5.12: *a: Amplitude data from 09:51:30 to 09:56:37 on day 209 of 2010, smoothed using a Lowess function and fitted with a spline smooth curve. b and c show the corresponding filtered H and D components of the magnetometer data.*

pulsations not being strong enough in amplitude to a cause a measurable Doppler shift.

5.4 Summary

In this chapter the design of the experiment to investigate the ability of the DPS-4D to observe Pc3 pulsations was described. The process of extracting data from the DFT files and results of the experiment were also discussed. Ionospheric Doppler oscillations observed at near-vertical incidences in F-region altitudes were compared with daytime Pc3 magnetic pulsations recorded simultaneously on the ground. However, no relationship was found between the two data sets.

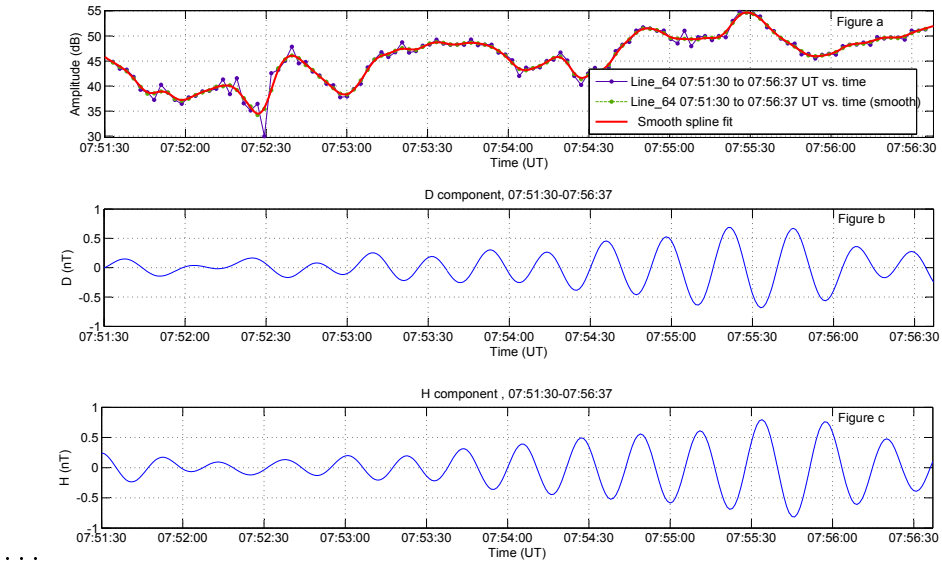

. . .

Figure 5.13: *a: Amplitude data extracted from DPS-4D recordings from 07:51:30 to 07:56:37 UT day 236 of 2010. b and c show high correlation between the H and D components with a peak- to-peak amplitude of 1.2 nT.*

Chapter 6

Conclusion and future work

6.1 Introduction

This chapter provides a summary of the results of the research and proposes future work. The aim of this study was to investigate and expand the capabilities of the new DPS-4D installed at Hermanus, South Africa in 2008. In particular, the investigation was centered upon whether the DPS-4D could provide data on Pc3 pulsations evident in the ionosphere.

6.2 Conclusion

This project was designed around the idea that, since the DPS-4D uses state-of-the-art technology to provide high resolution and accuracy, it may be possible to expand the capabilities beyond that of standard ionospheric sounding. The question was whether Pc3 pulsations could be observed with the DPS-4D. The results of the experiment show that although the DPS-4D is more advanced than its predecessors, it is not possible to observe Pc3 pulsations in the ionosphere with this instrument. This conclusion was reached based upon the fact that the expected relationship between the ground magnetometer data and ionospheric DPS-4D

data did not exist during the duration of the experiment. However, this conclusion should be evaluated within the context of the limitations of the experiment. These included:

- The non-continuous running of the Pc3 programme on the DPS-4D. This led to some of the active events going unobserved during the analysis process. In addition, this limitation also reduced the amount of analyzed data.
- The shortcoming in the programme that runs the CIT settings, which limited the amount of resolution that could be reached during the sounding process.

The experiment, however, did highlight a number of advantages of DPS-4D compared to its predecessors:

- The ability to operate in an RF noisy environment. This enhancement was made possible by the inclusion of the RIM technique (discussed in chapter 2) which greatly suppresses interferers, thereby increasing the SNR.
- Raw data access. In contrast to the earlier Digisondes , which outputted only Fourier-transformed data and didn't offer users the ability to design their own programmes, DPS-4D users can now design programmes and also get access to the "raw" data collected from the four receiver antennas in terms of the O and X polarisations. The two 16-bit quadrature samples for each sampled range and all

four receiver channels are stored. This feature makes it possible for DPS-4D users to process data with their own algorithms suitable for specific scientific research. In addition to the raw data access, a number of standard data products are also generated and stored by the DPS-4D. These include; vertical incidence ionograms, Doppler skymaps, daily directrograms, daily and hourly drift velocity plots and waterfall display plots.

- Continuous measurements. In the past Digisondes could only produce DFT files in 15-minute intervals. The DPS-4D offers the option of continuous sounding through the use of the ASAP option in the DCART software.

6.3 Future work

In this study the possible expansion of the DPS-4D capabilities was limited to the observation of Pc3 pulsations. However, other capabilities may be investigated in future, such as:

- Observation of ionospheric irregularities: These irregularities are due to electron density fluctuations within the ionospheric plasma. The HF coherent radars are sensitive to these fluctuations, thus they can be detected in the signal power at the receiver. Currently these irregularities are being detected by HF radar sounders installed around the world.

- Ionospheric tilt: In general, ionospheric tilt deflects a radio ray out of its great-circle plane. Upon returning to earth the ray is at an angle not that of the true bearing from a receiver to a transmitter. Using the DPS-4D as an HF radar system, the magnitude of error introduced by this tilt to the radio signals can be studied.

Therefore, the primary intention of this work is to explore the capabilities of the DPS-4D and expand on them with examples of science, which would help answer some of unknown features in ionospheric science.

References

Alperovich, L. S. and Fedorov, E. N.: Hydromagnetic waves in the magnetosphere and the ionosphere, pp. 52–53, Springer, Dordrecht, Netherlands, 2007.

Bibl, K.: Evolution of the ionosonde, Ann. Geophys., 41, 668–680, 1998.

Bourdillon, A. and Delloue, J.: Effects of geomagnetic pulsations on the Doppler shift of HF backscatter radar echoes, Radio Sci., 24, 183–195, 1989.

Chen, L. and Hasegawa, A.: A theory of long-period magnetic pulsations, 1. Steady state excitation of Field line resonance, J. Geophys. Res., 79, 1024–1032, 1974.

Cleveland, W. S.: Robust locally-weighted regression and smoothing scatterplots, J. Am. Stat. Assoc., 77, 829–836, 1979.

Engebretson, M. J., Meng, C.-I., Arnoldy, R. L., and Cahill, Laurence, J.: Pc 3 pulsations observed near the South polar cusp, J. Geophys. Res., 91, 8909–8918, 1986.

Greenwald, R. A., Baker, K. B., Dudeney, J. R., Pinnock, M., Jones, T. B, T. E. C., Villain, J.-P., C. J.-C., Senior, C., Hanuise, C., Hunsucker, R. D., Sofko, G., Koehler, J., and Nielsen, E.; Pellinen, R. W.-A. D. M. S. N. Y. H.: Darn/Superdarn: A global view of the dynamics of high-lattitude convection, Space Science Reviews, 71, 761–796, 1995.

Gupta, J. C. and Stening, R. J.: Period structure of Pc3, 4 micropulsations, Planet Space Sci., 19, 715–722, 1971.

Howard, T. A. and Menk, F. W.: Ground observations of high-latitude Pc3-4 ULF waves, J. Geophys. Res., 110, A04 205, 2005.

Jacobs, J. A., Kato, Y., Matsushita, S., and Troitskaya, V. A.: Classification of geomagnetic micropulsations, J. Geophys. Res., 69, 180–181, 1964.

Kelley, M.: The earth's ionosphere: plasma physics and electrodynamics, Academic Press, Burlington, MA, 2 edn., 2009.

Magnus, L.: Expanding the capabilities of DPS Ionosonde system, Master's thesis, Rhodes University, Grahamstown, 2001.

Margaret, G. K. and Russell, C. T.: Introduction to space physics, Cambridge University Press, Cambridge, 1995.

Marshall, R. A. and Menk, F. W.: Observations of Pc3-4 and Pi2 geomagnetic pulsations in the low-latitude ionosphere, Ann. Geophys., 17, 1397–1410, 1999.

McKinnell, L.: The progress of the South Africa ionosonde network, in: Radio Sounding and Plasma Physics, American Inst. of Physics, 2007.

Oppenheim, A. V. and Schafer, R. W.: Digital signal processing, Prentice-Hall, Englewood Cliffs, NJ, second edn., 1989.

Pearson, B.: Complementary code keying made simple, Tech. Rep. 1, Intersil corporation, FL 32905, AN9850, 2000.

Ponomarenko, P. V., Menk, F. W., Waters, C. L., and Sciffer, M. D.: Pc3-4 ULF waves observed by the SuperDARN TIGER radar, Ann. Geophys., 23, 1271–1280, 2005.

Reinisch, B., Huang, X., Galkin, I., Paznukhov, V., and Kozlov, A.: Recent advances in real-time analysis of ionograms and ionospheric drift measurements with digisondes, J. Atmos. Terr. Phys., 67, 1054–1062, 2005.

Reinisch, B. W.: Digisonde 4D system manual, University of Massachusetts Lowell Center for Atmospheric Research, Lowell, MA, 2009.

Reinisch, B. W., Haines, D. M., and Kuklinski, W. S.: The new portable digisonde for vertical and oblique sounding, Proc. AGARD EPP 50th Symposium, 502, 1– 11, 1992.

Reinisch, B. W., Scali, J. L., and Haines, D. M.: Ionospheric drift measurements with ionosondes, Ann. Geophys., 41, 695–702, 1998.

Reinisch, B. W., Galkin, I. A., Khmyrov, G. M., Kozlov, A. V., Bibl, K., Lisysyan, I. A., Cheney, G. P., Huang, X., Kitrosser, D. F., Paznukhov, V. V., Luo, Y., Jones, W., Stelmash, S., Hamel, R., and Grochmal, J.: New Digisonde for research and monitoring applications, Radio Sci., 44, RS0A24, 2009.

Royston, P.: Lowess smoothing, Tech. Rep. STB-3, Stata Technical Bulletin, Stata Corporation, Arizona, 1992.

Sutcliffe, P. R. and Poole, A. W. V.: Low latitude Pc3 pulsations and associated ionospheric oscillations measured by a digital chirp ionosonde, Geophys. Res. Lett., 11, 1172–1175, 1984.

Sutcliffe, P. R. and Poole, A. W. V.: Ionospheric Doppler and electron velocities in the presence of ULF waves, J. Geophys. Res., 94, 13 505–13 514, 1989.

Sutcliffe, P. R., DuToit, P. J., Julies, E. J. J., Pretorius, B. J., Theron, H., and Wright, D. R.: Collaborative effort to record cleaner geomagnetic pulsation data in South Africa., in: Xth IAGA workshop on geomagnetic observatory instruments, data acquisition, and processing, Hermanus, South Africa, 2002.

Tait, P.: Introduction to radar target recognition, The institution of engineering and technology, London, United Kingdom, 2009.

Takahashi, K., McPherron, R. L., and Terasawa, T.: Dependence of the spectrum of Pc 3-4 pulsations on the interplanetary magnetic Field, J. Geophys. Res., 89, 2770–2780, 1984.

Walker, A. D. M.: Magnetohydrodynamic waves in geospace: The theory of ULF waves and their interaction with energetic particles in the solar terrestrial environment, IOP, Bristol, 2005.

Walker, A. D. M., Greenwald, R. A., Stuart, W. F., and Green, C. A.: Stare Auroral radar observations of Pc5 geomagnetic pulsations, J. Geophys. Res., 84, 3373–3388, 1979.

Wright, D. M., Yeoman, T. K., and Chapman, P. J.: High-latitude HF Doppler observations of ULF waves. 1. Waves with large spatial scale sizes, Ann. Geophys., 15, 1548–1556, 1997.